

Callisto

Jeffrey M. Moore

NASA Ames Research Center

Clark R. Chapman, Edward B. Bierhaus

SouthWest Research Institute

Ronald Greeley, Frank C. Chuang, James Klemaszewski

Arizona State University

Roger N. Clark

U.S. Geological Survey, Denver

J. Brad Dalton

SETI Institute and NASA Ames Research Center

Charles A. Hibbitts

Dept. of Earth & Space Sciences, University of Washington

Paul M. Schenk

Lunar and Planetary Institute

John R. Spencer

Lowell Observatory

Roland Wagner

Institute of Space Sensor Technology & Planetary Exploration, DLR

17.1 INTRODUCTION AND OVERVIEW

Callisto, the size of Mercury, is underrated in comparison with its famous siblings. Were it a member of any other satellite system, it would be accorded due respect. While Callisto may be compared with Ganymede and Titan to illuminate how they have been modified, Callisto is a world in its own right, with unique surface processes, landforms, and evolution.

For more than a century before space age exploration of the Jupiter system, telescopic observers noted unambiguous surface markings on Io and Ganymede, while Callisto and Europa seemed rather featureless (Rogers 1995). Callisto was known to have the lowest albedo, with a relatively darker and redder leading hemisphere (Stebbins and Jacobsen 1928, Morrison *et al.* 1974). It was inferred, from its low density, that Callisto had a large H₂O component (Lewis 1972 a,b), but water was not readily detected spectroscopically, so its surface was thought to be mostly rocky (e.g., Morrison and Burns 1976). The *Pioneer* 10 and 11 Jupiter

encounters in the early 1970s contributed little new information about Callisto.

The 1979 *Voyager* encounters with the Jupiter system removed the burqua from Callisto. From size and mass determinations, its bulk density was refined to within 1% (e.g., Morrison 1982). Temperatures were measured of both the day and night sides (Hanel *et al.* 1979). Image resolutions approached 1 km/pixel (Smith *et al.* 1979 a,b), revealing a surface sculpted by impacts. Callisto was thus perceived as the archetype of geologic quiescence among the Galilean satellites, since the others exhibit widespread endogenic activity on their surfaces. Some dismissed Callisto as the most boring object of its size in the solar system.

Puzzles about Callisto remained after the *Voyager* encounters. For instance, is Callisto differentiated (e.g., McKinnon and Parmentier 1986, Schenk 1995)? Its optical surface composition remained enigmatic, though H₂O was finally positively detected (Clark and McCord 1980, Clark 1980). Limitations in resolution and coverage of *Voyager* imaging left subtle but important geological questions, such as whether small, smooth patches might be volcanic, or

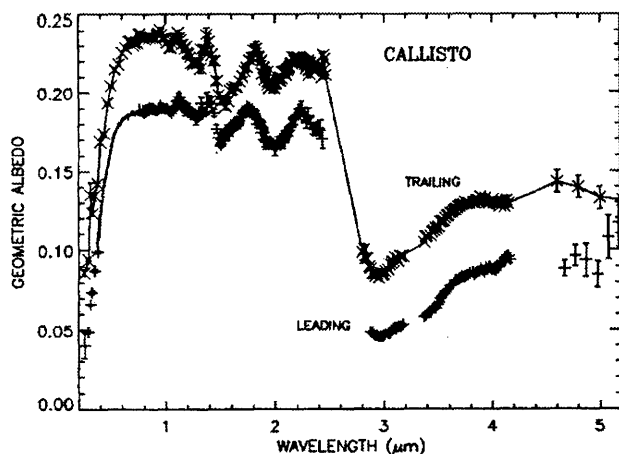


Figure 17.1. Reflectance spectra of Callisto 0.2–5 μm from earth-based observations (from Calvin *et al.* 1995).

whether the shallow relief of some craters resulted from plastic deformation (i.e., viscous relaxation) of bedrock (e.g., Schenk 1995).

Galileo observed Callisto during 12 targeted encounters from 1996 to 2001. The scientific objectives (Carr *et al.* 1995) of the Solid State Imaging (SSI) camera team were to examine the morphology (and origin) of (1) multi-ring structures, including associated scarps, troughs, and ridges; (2) palimpsests; (3) impact craters formed in icy targets; (4) catenae (crater chains); and (5) candidate endogenic deposits; and to study (6) areas not imaged or poorly imaged by *Voyager*; (7) the presence and mobility of volatile frosts at high latitudes; and (8) spectral indications of ice/silicate mixtures. The Near Infrared Mapping Spectrometer (NIMS) acquired data in up to 408 spectral channels with resolutions sometimes <1 km/pixel. Many NIMS and SSI observations were coordinated to provide complementary context. Thermal measurements of Callisto at various latitudes and times of day were made by the Photopolarimeter Radiometer (PPR). Callisto's gravity was measured by radio tracking of *Galileo*, and magnetometer data provided insight concerning Callisto's interior (Anderson *et al.* 1998, 2001, Khurana *et al.* 1998, Kivelson *et al.* 1999). In December 2000, the *Cassini* spacecraft, en route to Saturn, passed near Jupiter and observed Callisto with several instruments.

In this chapter, we first discuss the properties and composition of Callisto's uppermost surface before reviewing landforms. Such properties are among the most distinguishing features of Callisto and from which (along with interior properties) inferences about its evolution are most directly derived. Other chapters specifically deal with satellite origins (Chapter 2), interiors (Chapter 13), cratering morphology, statistics and inferred surface ages (Chapter 18). Briefly, Callisto formed as part of the Galilean satellite system, with a primordial composition reflecting its position in the proto-Jovian nebula. Its interior is only partially differentiated and it is the most thoroughly cratered Galilean satellite, constraining evolutionary histories. Several recent studies of Callisto (e.g., Schenk 1995, Moore *et al.* 1999, Greeley *et al.* 2000), have been modified, updated, and integrated for this synthesis of the state of Callisto knowledge as of 2003.

17.2 SURFACE LAYER PROPERTIES AND COMPOSITION

17.2.1 Spectrally-Inferred Composition

Callisto's optical surface consists of water ice, various unidentified hydrated materials/minerals, and trace amounts of CO_2 (perhaps as fluid or gaseous inclusions) and SO_2 . The hydrated non-ice material(s) are generally dark, exhibiting weak ultraviolet Fe^{3+} absorptions and a positive visible-to-near-IR slope, like some carbonaceous chondrites (Clark 1980). CO_2 and other trace constituents are also present, though it is unclear if they occur in the ice as well (Hibbitts *et al.* 2001a). There is strong evidence for Mg-OH-bearing phyllosilicates (e.g., clays), but specific minerals cannot be uniquely identified with existing spectral resolution. There are also some other small, unidentified absorptions in Callisto's spectrum. Figure 17.1 shows an example of Callisto's full-disk reflectance spectrum from 0.2 to 5 μm (Calvin *et al.* 1995, which is an excellent review of pre-1995 work).

H₂O Ice and Non-Ice

Infrared spectra of Europa, Ganymede, and Callisto show water ice absorptions at 3.0, 2.0, 1.5, 1.25, and 1.04 μm . Pilcher *et al.* (1972) identified H_2O on some of the satellites. Kieffer and Smythe (1974), comparing with spectra of CH_4 , CO_2 , H_2O , H_2S , NH_3 , and NH_4SH frosts, found H_2O as the dominant component on Europa and Ganymede, with upper limits of 5 to 28% for other frosts, based on linear combinations (i.e., assuming areal mixtures). They concluded that other materials must be present on Callisto. Pollack *et al.* (1978) determined the fractional amounts of water-ice coverage on Ganymede's trailing and leading sides and Europa's leading side as $50 \pm 15\%$, $65 \pm 15\%$, and $\geq 85\%$, respectively, and interpreted Callisto's 2.9 μm band as due primarily to bound water in non-ice surface materials.

Different ice absorption bands can be modeled as indicators of ice grain size and/or ice purity in the context of contaminants (Clark 1981, and Clark and Lucey 1984). The strong OH fundamental near 3 μm can be produced by small amounts of ice while the weak 1.04 μm combination band can indicate a long (mm to cm) path length. Clark *et al.* (1980) obtained spectra of all Galilean satellites and found the 1.04 μm band in Callisto's spectrum; it is 2.4% deep in the hemispheric spectra, indicating abundant water ice or lesser amounts of large-grained ice. Abundant ice would make the depth of the strong 3 μm band $\sim 99\%$, but it is only $\sim 70\%$. Thus either there are ice-poor regions on the surface or the H_2O ice surface has a fine sub-micron structure that scatters some photons before they are absorbed. A very fine (<1 μm) surface structure on an H_2O ice block, or fine grains coating larger grains, might show a weak 3 μm absorption while still allowing photons at other wavelengths to penetrate deeper into the surface resulting in relatively strong ice absorptions. Such grains would have to be <1 μm and a total optical path in H_2O ice of ~ 1 μm would be required (see Clark and Lucey 1984). A problem is that water molecules constantly migrate on Callisto's surface, due to the ice's significant vapor pressure at ~ 167 K, resulting in grain growth that fills in fine surface structure (Stephenson 1967, Kieffer 1968, Hobbs, 1974, Clark *et al.* 1983, 1986,

Dalton 2000, Spencer 1987a). Small grains would grow to $\sim 1 \mu\text{m}$ in only a few years and to 1 mm in 10 Myr (Clark *et al.* 1983). Thus, Callisto apparently has some fairly pure water ice patches (indicated by the $1.04 \mu\text{m}$ ice band) and some patches of the surface that are ice-free, consistent with more recent *Galileo* SSI imaging.

Calvin and Clark (1991) successfully modeled Callisto's $0.2\text{--}4.1 \mu\text{m}$ reflectance spectrum using a simultaneous intimate-plus-areal-mixture solution of H_2O ice and dark material. The best fit has 20–45 wt% H_2O ice in the optical surface with a fairly large-grained ice component; spectral features beyond $\sim 2.5 \mu\text{m}$ are attributed to non-ice hydrated materials/minerals. Mathematically removing the ice absorptions from Callisto's spectrum reveals the non-ice spectral component, which shows absorptions suggesting hydrated silicates bearing both oxidation states of iron (Fe^{2+} , Fe^{3+}); some features match mixtures of Fe- and Mg-end member serpentines with remaining discrepancies due to other, possibly opaque, phases. Carbonaceous chondrites, which have Fe-serpentines, may be a candidate for Callisto's non-ice material. Inconsistencies remain among (a) Calvin and Clark's (1991) non-ice model, (b) laboratory spectra of Mg- and Fe-serpentines (King and Clark 1989), and (c) carbonaceous chondrite spectra. Another discrepancy is that the calculated serpentine mixture is much brighter than the Callisto non-ice material between 1.5 and $2.2 \mu\text{m}$, conceivably due to the presence of other matrix phases or opaque materials. Signal-to-noise limitations in Callisto spectra hide weak infrared features that might otherwise resolve these issues.

Calvin and Clark's (1991) best match involved two ice components, one with mm–cm grains, the other with grains $200\text{--}500 \mu\text{m}$. The non-ice grains must be $>50\text{--}100 \mu\text{m}$ in order to avoid suppressing the weaker ice bands in calculated spectra. The best-fitting models have patches of intimately mixed ice and rock, and patches of pure rock with up to 70% coverage. Roush *et al.*'s (1990) models of the $3 \mu\text{m}$ region involve mixtures of either ice and serpentine, or ice, magnetite and serpentine, suggesting that magnetite can suppress the 2.2 and $2.4 \mu\text{m}$ serpentine features; their best fits involved large-grained ice. Calvin and Clark (1993) suggest that a small amount of fine-grained ice is on the leading hemisphere. They also found hints of a $3.1 \mu\text{m}$ feature possibly indicating NH_3 on Callisto, but neither *Galileo* NIMS nor *Cassini* Visual and Infrared Mapping Spectrometer (VIMS) data analyzed so far show this feature.

Figure 17.2 shows representative “icy” and “non-icy” spectra from *Galileo* NIMS. “Non-icy” spectra are darker, but both show ice absorptions. Areal mixing of H_2O ice and “non-ice” occurs on scales below a few km, the best NIMS resolution. Indeed, *Galileo* SSI images show light and dark patches at scales of tens of meters and areal mixing may even exist at centimeter scales (Spencer 1987b). Carlson *et al.* (1996) discovered the CO_2 absorption on Callisto. A few NIMS spectra show a $2.3 \mu\text{m}$ absorption (Figure 17.3), indicative of Mg–OH bearing minerals, consistent with models that use serpentine. C–H bonds would be possible, instead, but the associated, stronger CH stretching fundamental absorptions in the $3.2\text{--}3.4 \mu\text{m}$ region are not evident, or at least not strong enough to account for the $2.3 \mu\text{m}$ band; possibly there are organic compounds on Callisto, despite the weakness of the CH fundamental features (McCord *et*

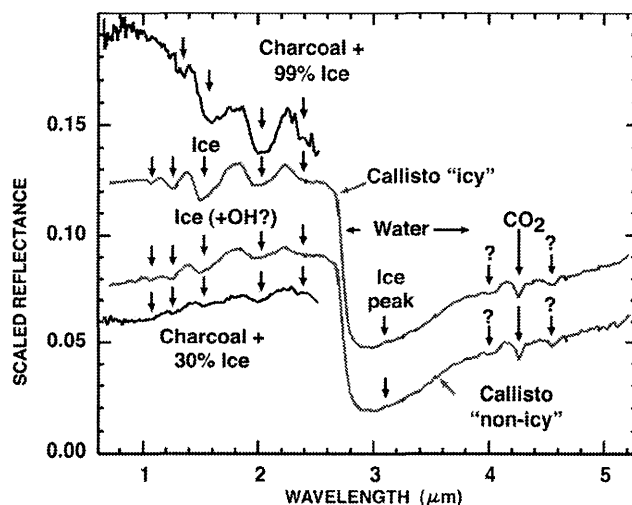


Figure 17.2. *Galileo* NIMS “icy” and “non-icy” spectra of Callisto.

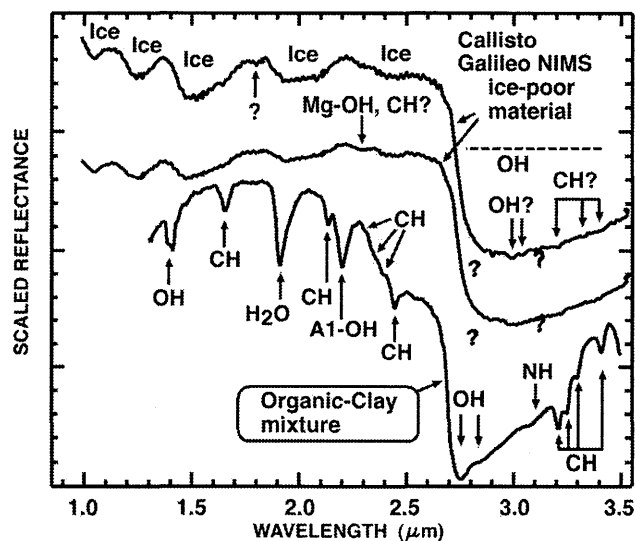


Figure 17.3. *Galileo* NIMS spectra show $2.3 \mu\text{m}$ absorptions, typical of Mg–OH bearing minerals. Other possible weak features may be due to CH.

al. 1997, 1998). NIMS spectra show no hint of a sharp OH stretch fundamental near $2.72 \mu\text{m}$, which would confirm a crystalline phyllosilicate mineralogy; perhaps the serpentine is amorphous as in carbonaceous chondrites (Browning *et al.* 1991). So, after *Galileo*, we can say only that the non-icy material is consistent with Fe^{2+} , Fe^{3+} , and Mg–OH bearing minerals.

McCord *et al.* (1997, 1998) analyzed absorptions at 3.4 , 3.88 , 4.05 , 4.25 , and $4.57 \mu\text{m}$ and suggested C–H, S–H, SO_2 , CO_2 , and C–N as candidate molecules. While some CO_2 -bearing igneous and metamorphic minerals absorb in the $3.7\text{--}5 \mu\text{m}$ region (eFigure 17.1, see appendix on the accompanying CD), they are unlikely on such a geologically inactive body as Callisto. The features could be related to orientation effects of CO_2 molecules incorporated into some other host phase.

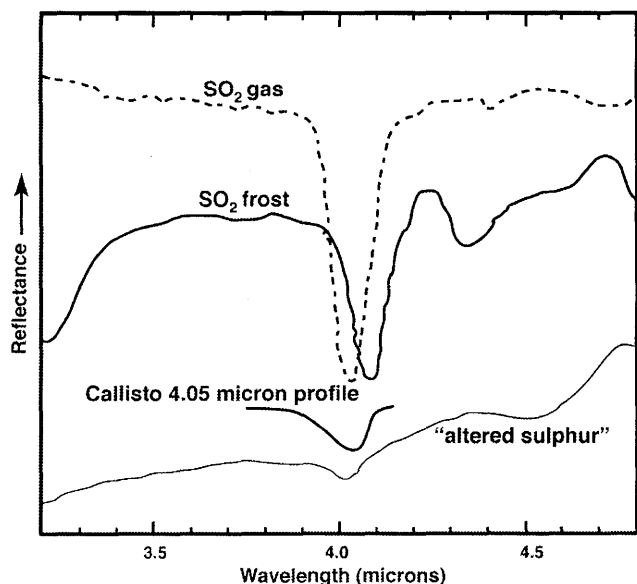


Figure 17.4. The reflectance spectra of SO₂ gas, adsorbed SO₂, and SO₂ frost are shown (from Fanale *et al.* 1979) along with the average profile of the 4 μm feature in Callisto spectra (modified from Figure 17.15, McCord *et al.* 1998).

Sulfur Dioxide

A characteristic broad, shallow 0.28 μm sulfur dioxide absorption band was co-discovered on Callisto with the Hubble Space Telescope (HST) (Noll *et al.* 1997) and the International Ultraviolet Explorer (IUE) (Lane and Domingue 1997), and later confirmed with the *Galileo* Ultra-Violet Spectrometer (UVS) (Hendrix *et al.* 1998). *Galileo* NIMS data (McCord *et al.* 1998) revealed a broad feature (Figure 17.4), centered near 4.05 μm , extending from ~ 3.92 to ~ 4.10 μm , consistent with SO₂, but not with the much narrower features due to pure SO₂ frost or gaseous SO₂ as found on Io (Fanale *et al.* 1979, Smythe *et al.* 1979). With a vapor pressure of ~ 0.01 mbar, pure SO₂ would sublime at Callisto's surface pressure and temperature. McCord *et al.* (1998) proposed that the SO₂ exists in a physical state similar to the CO₂ on Callisto, as molecules trapped in host materials at Callisto's optical surface. But the origins of CO₂ and SO₂ on Callisto must not be related, since they are distributed very differently around Callisto (McCord *et al.* 1998, Hibbitts *et al.* 2000).

Variable strength of the 4.05 μm absorption band around Callisto suggests a degree of stability of SO₂ over geologic timescales, but it also may be affected by magnetospheric and impact processes. It is consistently more abundant on Callisto's leading side (Hibbitts *et al.* 2000), implying that implantation of sulfur ions is not responsible for Callisto's SO₂. Lane and Domingue (1997) invoked the effect of parallax: neutral sulfur atoms streaming radially away from Jupiter would preferentially impact the leading side, consistent with *Galileo* UVS data showing that the anti-jovian quadrant of the leading hemisphere (containing Asgard) has very little, if any, SO₂ (Hendrix *et al.* 1998). According to Hibbitts *et al.* (2000), however, NIMS data show that the absorber is under-abundant in the Asgard and Valhalla impact basins, but is not asymmetrically dis-

tributed between the Jupiter-facing and anti-jovian quadrants. There are hints in the generally mottled distribution of SO₂ at one to tens of km scales of correlations with deep impact craters, but the correlation is too poor to define a genetic relation. In summary, SO₂ is neither gas nor solid on Callisto, but likely exists as molecules trapped in surficial (and perhaps subsurficial) materials. It may be primordial or evolved from processes within Callisto, but is probably not exogenic in origin.

Carbon Dioxide

Carbon dioxide is another minor constituent on Callisto's surface. NIMS first revealed its 4.25 μm feature (Carlson *et al.* 1996). Later, *Cassini* VIMS also detected CO₂ in disk integrated (sub-pixel) observations of Callisto (McCord *et al.* 2001). Its presence is further substantiated by detection of emission lines of molecular CO₂ in a tenuous $\sim 10^{-12}$ bar exosphere (Carlson 1999). Like SO₂, the CO₂ absorption band's characteristics are inconsistent with frost or gas, but may be explained by molecules trapped in a host material (McCord *et al.* 1998) (e.g., in gaseous or fluid inclusions). The center wavelength is ~ 0.1 μm short of that of either amorphous or crystalline frost. Since CO₂ ice is even less stable than SO₂ ice, having vapor pressures of 0.04, 1.8, and 3.1 mbar at 120, 140, and 160 K, respectively (James *et al.* 1992), CO₂ frost would not be stable on Callisto. Analysis of NIMS data over four years finds the spectral characteristics of the CO₂ absorption are constant (Hibbitts *et al.* 2000), perhaps a single material serves as the host for CO₂ on Callisto.

According to McCord *et al.* (1998) and Hibbitts *et al.* (2000), the global distribution of CO₂ is asymmetric (Figure 17.5), with more CO₂ on the trailing side (opposite to the trend for SO₂). Superimposed on the global pattern are areas with more CO₂, invariably associated with morphologically fresh impact craters and with the freshest ejecta (e.g., young impact craters within the Asgard Basin; Hibbitts *et al.* 2002). The distribution of CO₂-rich impact craters is extensive, without longitudinal dependence; it suggests a transient existence for the CO₂, first lost from the icy ejecta and then from the crater itself until an equilibrium concentration is reached; the loss may help refresh the tenuous CO₂ exosphere.

Association of CO₂ with fresh craters suggests that it originates in the bedrock and is slowly lost as it sublimates away, which is consistent with the mechanism proposed by Moore *et al.* (1999) to explain the extensive mass wasting observed on Callisto. However, although there may be CO₂ ice in Callisto's bedrock, all CO₂ detected by NIMS is in the non-ice material. The water ice outside the polar regions of Callisto, including the bright impact craters and ejecta, is essentially black from ~ 3 to 5 μm , so none of the observed CO₂ band at ~ 4.26 μm could be due to the presence of CO₂ in the ice (Figure 17.6), assuming that the ice and non-ice materials are in discrete patches and thus mix linearly (Spencer 1987b). Assuming that all CO₂ detected by NIMS is in the non-ice material, Hibbitts *et al.* (2002) estimate that only $\sim 0.1\%$ by weight of CO₂ in the optical surface could account for the observed band.

In considering the origin of CO₂ on Callisto, it is instructive to compare with Ganymede, which has surficial

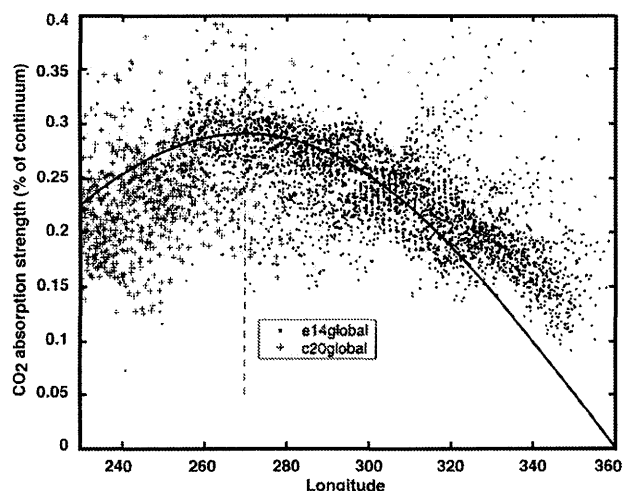


Figure 17.5. A scatterplot of CO₂ band depth versus longitude for global-scale observations.

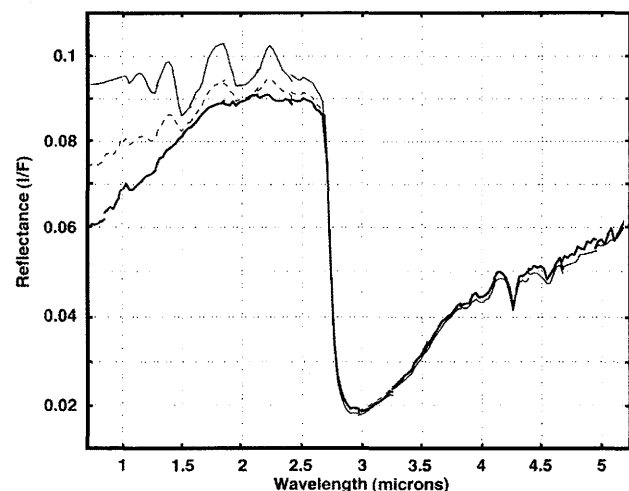


Figure 17.6. Reflectance spectra from the NIMS C3ARINGS observation of an impact crater and surrounding terrain near Asgard Basin on the anti-jovian portion of the leading hemisphere.

CO₂, very likely hosted in its non-ice material but which is distributed very differently across its surface. There are no CO₂-rich impact craters on Ganymede (Hibbitts *et al.* 2001b), showing that the impactors striking both moons are not the source of the CO₂. Hence, Callisto's subsurface is richer either in CO₂ or CO₂-precursor materials than Ganymede's, consistent with Callisto's less evolved interior (Anderson *et al.* 1998). If the CO₂ is primordial, impact craters may be excavating CO₂-rich primordial material that is in equilibrium with the greater confining pressures; once exposed to the surface, some CO₂ is released until reaching a new equilibrium concentration. The absence on Ganymede of Callisto's leading/trailing side dichotomy of CO₂ suggests that magnetospheric particles that cannot penetrate Ganymede's dipole field are somehow responsible for the increased abundance on Callisto. O⁺ ions may be combining with C-bearing, perhaps carbonaceous chondritic, non-ice surficial materials (e.g., Johnson and Fanale 1973, Calvin and Clark 1991) to create CO₂ in the non-ice material.

Irradiation of surface water ice cannot produce the required CO₂ since it would need to migrate into the non-ice material before escaping to space, which would be difficult for discretely mixed ice and non-ice materials; moreover, it is the less icy areas that show more carbon dioxide. Alternatively, irradiation may work indirectly by modifying non-ice materials in ways that enable it to more efficiently trap primordial CO₂ escaping from the subsurface.

17.2.2 High-Energy Particle and Dust Environment

Callisto is embedded in the jovian magnetosphere and bombarded by trapped energetic particles. It is also bombarded by outward-spiraling neutral atoms and by interplanetary and jovian-system dust. Though only a solar system background level of micron-sized dust impacts Callisto (Colwell *et al.* 1998), nanometer-sized dust coupled to Jupiter's magnetic field is at 20 to 1000 times background levels (Grün *et al.* 1998). Even at these levels, though, only nanometers would accumulate on the surface of Callisto over millions of years. However, energetic charged particles, primarily 20 keV to 100 MeV protons, O²⁺, and S³⁺ ions and 20 to 700 keV electrons, can greatly affect the upper microns to millimeters of the surface (Geiss *et al.* 1992, Cooper *et al.* 2001). Heavy ions (Oⁿ⁺ and Sⁿ⁺) and solar UV radiation affect the upper micron while proton energy deposition dominates at several microns. At deeper levels, electrons have the greatest effect on chemistry (Johnson 1990). Ion and proton irradiation modifies UV and VNIR spectral traits, while effects of electronic ionization are revealed by mid- and thermal-IR spectroscopy. Thus, specific remote sensing techniques address particular styles of surface irradiation. Iogenic neutral atoms deliver negligible energy ($\sim 10^4$ or 10^5 keV cm⁻²s⁻¹, on the order of meteoroid impacts); but their effects could accumulate with time (Cooper *et al.* 2001).

Because Callisto is the furthest large moon from Jupiter, its flux of energetic particles is lowest (about two orders of magnitude less than for Europa). However, its surface is fully exposed to the charged particles, unlike Ganymede's that is partially shielded by an internally driven magnetic field (plasma particles ≥ 10 keV may still penetrate Ganymede's field). Callisto's total flux of energetic (> 20 keV) particles is similar to that at the equatorial region of Ganymede, ~ 2 to 3×10^8 keV cm⁻²s⁻¹ (Cooper *et al.* 2001). Lower-energy co-rotating electrons and ions have small gyroradii and may strike the trailing hemisphere with little deviation, unless there is a significant magnetospheric interaction with Callisto's tenuous ionosphere (Kliore *et al.* 2001). However, higher energy particles (mostly higher charged ions) with greater gyroradii distribute their bombardment more fully towards Callisto's leading hemisphere. Much lower energy particles have gyroradii equal to the body's radius for Callisto than for the other Galilean moons (Cooper *et al.* 2001), so they have a greater global component on Callisto and thus make up a greater proportion of the particles striking the trailing hemisphere. However, the peak flux on to the trailing side may still be up to an order of magnitude greater than elsewhere and several times the globally average flux (Cooper *et al.* 2001).

The energies of these particles are sufficient to cause many chemical reactions in the surface. Theoretical model-

ing by Delitsky and Lane (1998) predict creation of complex products from the irradiation of CO₂-rich ices with Sⁿ⁺ and Oⁿ⁺ ions. In one reaction, the stopped Sⁿ⁺ could combine with freed O to form SO and SO₂. Meanwhile, electrons react with water molecules to form species such as H₂O⁺, H₃O⁺, and H₂O₂ (Geiss *et al.* 1992; Delitsky and Lane 1997). These may be end products or they can act as intermediaries in producing O₂ (Sieger *et al.* 1998). Proton irradiation of O₂ or CO₂-bearing ice may also create H₂O₂ (Moore and Hudson, 2000). A UV absorption attributed to H₂O₂ has been detected on Callisto's leading side (Hendrix *et al.* 1999). However, O₂ has yet to be detected on Callisto.

A 4.57 μm absorption band (C-N) in spectra of less icy regions (McCord *et al.* 1998) may indicate organic solids such as tholins on Callisto. Ice-bearing tholins can be created from the irradiation of CH₄/NH₃/H₂O gases and from ice mixtures containing water/methanol/carbon dioxide/ethane ices (McDonald 1991, McDonald *et al.* 1996). Stopped Oⁿ⁺ magnetospheric ions could combine with carbon (or sulfur) in the non-ice material to form volatile CO and CO₂ (SO and SO₂). Because the stable state of these molecules on Callisto is gaseous, they must be trapped in the non-ice material to remain on the surface. More laboratory work is needed to investigate chemistry that occurs during the irradiation of Callisto-like non-ice materials.

17.2.3 Regolith and Surface Texture

Callisto is large enough to have retained surficial water ice despite its low albedo and consequent high surface temperature. Its surface may behave like a comet's in some ways, with lag deposits resulting from sublimation of volatiles, but gravity has presumably played a more important role, and the albedo of its dominant non-ice surface component is higher than known comet albedos. Information on Callisto's surface texture is obtained from various remote sensing techniques, including photometry, photopolarimetry, thermal emission, and radar.

Photometry and Polarimetry

Early disk-integrated, low phase angle photometric and polarimetric studies of Callisto are summarized in Morrison and Morrison (1977) and Veverka (1977a,b). Callisto's geometric albedo (0.22 including the opposition effect) is less than half that of Ganymede, and its bolometric albedo is ~0.11 (Buratti 1991). Away from opposition, the trailing side is ~12% brighter than the leading side (opposite the pattern on the other Galilean satellites), despite the fact that the leading side includes the large, relatively bright impact basins Valhalla and Asgard. Callisto's opposition effect is larger than that of the other icy Galileans; it is so much larger on the leading side that, at zero phase angle, the two hemispheres are almost equally bright.

Polarization shows striking leading/trailing asymmetries, with the leading side being lunar-like (large-amplitude negative branch, inversion angle ~20°) and the trailing side resembling Ganymede and Europa (lower amplitude negative branch, inversion angle ~12°). Callisto lacks a negative polarization spike at the very low phase angles where the opposition surge is seen (Rosenbush *et al.* 1997), unlike Europa

and Ganymede, perhaps due to larger silicate grains on Callisto. Preliminary analysis of high phase angle polarization data from the *Galileo* PPR (Martin *et al.* 2000), shows polarization peaking near 5% at 6800 Å at phase angles near 100°, comparable to the brightest lunar regions (Dollfus and Bowell 1971).

Buratti (1991) believes the photometry implies that regolith on Callisto's trailing side is more compact than on the leading side, while Domingue *et al.* (1997), utilizing opposition effect data from Thompson and Lockwood (1992), reach the opposite conclusion. In general, Callisto's photometric and polarimetric behavior is more lunar-like than that of Ganymede and Europa, especially its leading hemisphere. The leading side suffers more micrometeorite bombardment but less magnetospheric charged particle sputtering than the trailing side, though the role played by these distinctions in causing observed hemispheric dichotomies remains unclear.

Thermal Characteristics

Callisto is the warmest Galilean satellite, with a disk-integrated brightness temperature ~158 K at 20 μm (Morrison 1977, adjusted to the now-accepted radius of 2409 km, Davies *et al.* 1998) and mean subsolar temperatures near 165 K (Figure 17.7). Predawn equatorial nighttime temperatures are 80 ± 5 K (Hanel *et al.* 1979, Spencer 1987b), with regional variations. The diurnal temperature range implies a thermal inertia ~5 × 10⁴ erg cm⁻² s^{-1/2} K⁻¹ (SI units = 50 J m⁻² s^{-1/2} K⁻¹), strikingly similar, considering different surface compositions, to ~7 × 10⁴ for Ganymede and Europa (Spencer 1987b, Spencer *et al.* 1999). Eclipse cooling curves show that Callisto's surface is inhomogeneous, including a lower thermal inertia component responsible for rapid initial cooling and a higher thermal inertia component producing slower cooling later during the eclipse, which Morrison and Cruikshank (1973) explained with a 2-layer model in which a low thermal inertia component up to a few millimeters thick overlies a higher thermal inertia layer; alternative solutions involve two components separated horizontally (Spencer 1987b). Either way, there is some extremely uncompact surface material, with thermal inertia ~1.5 × 10⁴ erg cm⁻² s^{-1/2} K⁻¹.

Callisto's thermal emission spectrum as measured by *Voyager* IRIS is featureless, offering no clues to surface composition (see Appendix A). However, Callisto is not a blackbody, as brightness temperatures (T_B , defined as the temperature of a blackbody emitting the same radiance at a given wavelength) of disk-resolved spectra vary significantly with wavelength, probably due to unresolved temperature contrasts; warmer parts of the surface contribute more of the radiance at shorter wavelengths, resulting in increasing T_B with decreasing wavelength. This T_B slope varies strikingly with solar incidence angle (Spencer 1987b, and Figure 17.8), being greatest in near-terminator sunlit spectra due to oblique illumination of topography causing local temperature contrasts. But, enigmatically, slopes are also high in nighttime spectra. The T_B slopes of Ganymede spectra, in stark contrast, show almost no variation with solar incidence angle, suggesting a much smoother surface and smaller near-terminator temperature contrasts.

Thermal emission from deeper in the surface, for which daytime brightness temperatures are lower, is measured at

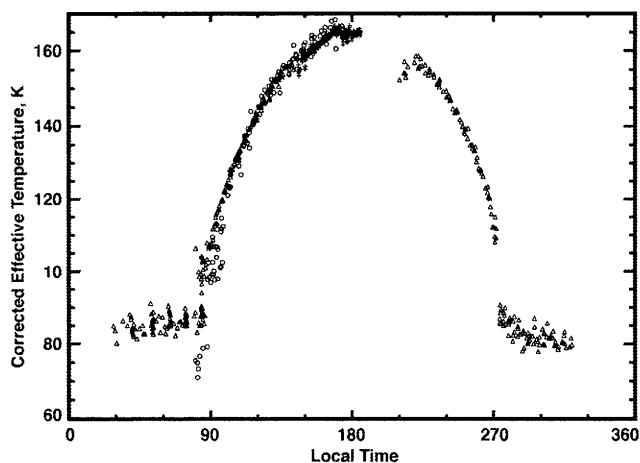


Figure 17.7. Equatorial effective temperature profile for Callisto, assembled from *Galileo* PPR data. Observations $<30^\circ$ from the limb are excluded. Circles: C3 encounter, $37\ \mu\text{m}$, subsolar longitude 113°W . Triangles: C10 encounter, $17\ \mu\text{m}$, subsolar longitude 72°W . Crosses: C21 encounter, $21\ \mu\text{m}$, subsolar longitude 24°W . All measurements are adjusted to a heliocentric distance of 5.2 AU and to a solar phase angle of 30° , assuming a disk-resolved thermal phase coefficient equivalent to a 0.12% brightness temperature change per degree, derived for Ganymede from the *Voyager* Infrared Interferometer Spectrometer (IRIS) observations (Spencer 1987a). Brightness temperatures, which are wavelength-dependent, are converted to effective temperatures (the temperature of a blackbody emitting the same total power) using the shapes of representative *Voyager* IRIS spectra: a subsolar spectrum is used to convert daytime temperatures, and a pre-dawn spectrum is used to convert nighttime temperatures. Note that C10 post-sunset temperatures are colder than C10 pre-dawn temperatures, which themselves increase towards dawn and are warmer than C3 pre-dawn temperatures, indicating regional variations in nighttime temperature that are unrelated to local time.

submillimeter and longer wavelengths. At $0.355\ \text{mm}$, Callisto's brightness temperature is $135 \pm 11\ \text{K}$ (de Pater *et al.* 1989), dropping to $\sim 90\ \text{K}$ beyond $2\ \text{mm}$ (Muhleman and Berge 1991, and references therein), consistent with expected temperatures below the diurnal skin depth, suggesting emissivity near unity even in the microwave. Recently, the Infrared Space Observatory (ISO) bridged the gap between *Voyager* IRIS and ground-based radio observations, obtaining a $50\text{--}180\ \mu\text{m}$ spectrum of Callisto (Burgdorf *et al.* 2000).

Callisto's daytime thermal radiation is completely dominated by the dark, non-ice surface component, due both to its higher temperature and areal dominance. Thus traits of the icy component – unresolved in even the highest resolution *Galileo* PPR data – remain largely unknown, although they determine sublimation rates. The daytime temperature of the icy component on the leading side is estimated to be $114 \pm 17\ \text{K}$, using the temperature dependence of the near-IR water-ice reflectance spectrum (Grundy *et al.* 1999).

Radar Characteristics

Callisto's radar signature is unusual, although not as extreme as for Ganymede and Europa. Its radar geometric albedo at 13 and $3.5\ \text{cm}$ is ~ 0.18 (Ostro *et al.* 1992), com-

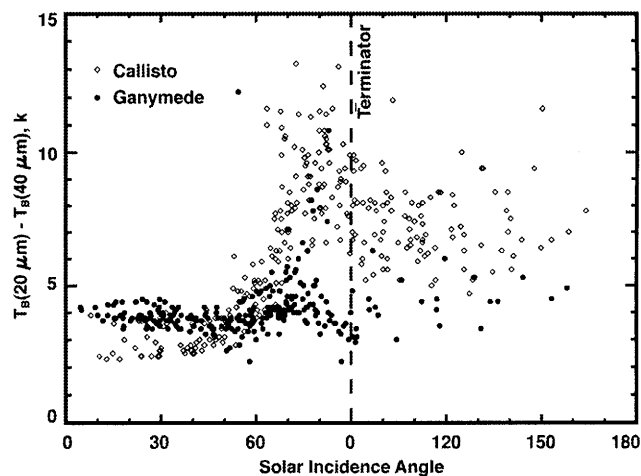


Figure 17.8. Brightness temperature (T_B) wavelength slope (in kelvin), measured by the difference between $20\ \mu\text{m}$ and $40\ \mu\text{m}$ T_B , as a function of solar incidence angle, for *Voyager* IRIS spectra of Callisto and Ganymede, adapted from Spencer (1987a). Spectrum slope may measure the amplitude of unresolved temperature contrasts within the IRIS field of view. The steep slope of near-terminator Callisto spectra probably results from temperature contrasts associated with rough topography. Ganymede's surface is apparently much smoother at thermally-significant length scales, and does not show this effect, except near the south pole, where all the high-slope Ganymede spectra were obtained.

pared with 0.025 for a typical terrestrial planet, and its circular polarization ratio is 1.2 compared with 0.1. Callisto shows no detectable specular component and there is no significant radar difference between Callisto's leading and trailing hemispheres (Ostro *et al.* 1992). Crude delay-doppler images (Ostro *et al.* 1992) and imaging of the radar return using the Very Large Array (Harcke *et al.* 2001), are possible, but insufficient for detailed correlation with geological features. At $70\ \text{cm}$, albedo is unusually high, but lower than at shorter wavelengths (Black *et al.* 2001a). These unusual properties probably result from near-surface material being only weakly absorbing, allowing for multiple scattering in the subsurface, whereas single-scattering from the surface dominates radar reflectivity of terrestrial bodies. Coherent backscattering explains the circular polarization ratios (Hapke 1990, Peters 1992). Black *et al.* (2001b) reproduce Callisto's scattering behavior with a model surface of icy particles ranging to $>1\ \text{m}$ in size, distributed in a matrix of porous water ice a few meters thick. The high surface albedos rule out silicates as the scattering particles.

The ice-rich regolith implied by radar data contrasts with the photometric, imaging, and spectroscopic results, which suggest a surface mostly covered with dark, non-volatile, ice-free material, with only occasional exposures of water ice on topographic highs. Perhaps the ice-free material seen optically is unusually radar-transparent or less than a few cm thick, and overlies the ice-rich regolith that dominates the radar signature. The model of a cm-thick non-ice ("dusty") layer overlying an icy regolith is nicely consistent with the 2-layer thermal models of Morrison and Cruikshank (1973). A thin dust layer should result from thermal segregation (Spencer 1987b), in which ice sublimates until a non-volatile lag deposit develops that is just thick enough

to greatly limit sublimation, both by physically blocking gas escape and by insulating the underlying ice from the 165 K noontime temperatures.

However, the smoothness of much of Callisto's surface on a scale of tens of meters, gives the impression of a layer many meters thick. Perhaps much of Callisto's surface is analogous to the pediments produced by erosion in arid climates on Earth, where a smooth bedrock surface is produced by erosion of a mountain front, and is protected from further erosion by a thin layer of surface debris, whose smoothness gives the impression of greater thickness (e.g., McGee 1897). A pediment-like surface might result from recession of steep slopes by sublimation erosion (Moore *et al.* 1999), although this process would not obviously yield large areas covered in dust only centimeters thick. Of course, large areas of much greater dust thickness would contribute negligibly to the radar signature: Callisto's radar albedo is 1/3–1/4 that of Europa, so conceivably 2/3 to 3/4 of its surface could be covered in thick, radar-dark dust, with the remainder having a Europa-like albedo. However, some mechanism, like an extremely porous surface with porosity gradually decreasing with depth (G. J. Black, personal communication 2002), would be needed to suppress a specular return from the thick dust regions.

17.3 GEOLOGY

The geology of Callisto calls to mind the dance-hall wallflower, who at a distance appears unremarkable and unassuming, but upon close examination reveals unexpected charm (Figures 17.9, 17.10, and 17.11). Globally, Callisto appears to be just a sphere covered by impact craters. In this review of Callisto's geology, we start with the smallest, most intriguing features, then examine progressively larger landforms and terrains.

At the smallest scales imaged by *Galileo*, Callisto is remarkable. Kilometer-scale craters on Callisto seen at < 50 m/pixel (Figure 17.12) range from those with continuous, sharp-crested bright rims and bowl-like interiors to those whose raised rims have become very discontinuous and with shallower interiors (Moore *et al.* 1999, Basilevsky *et al.* 2000). The rim material appears to disaggregate in a manner that resembles decomposition of the rim-forming bedrock itself rather than pulverization by small impacts. The loose fine-grained dark material may be a byproduct of rim-forming bedrock disintegration. In contrast, kilometer-scale craters on Ganymede's dark terrain (Figure 17.13) show a range of morphologies generally due to modification by the subsequent rain of mostly smaller impacts (e.g., Prockter *et al.* 1998a), as had been anticipated pre-*Galileo* for both Callisto and Ganymede's dark terrains. Instead, Callisto's crater rims appear to disaggregate by decomposition of the rim-forming bedrock itself rather than by pulverization by small impacts. The lower-lying undulating dark plains may be a byproduct of bedrock disintegration.

Disintegration of smaller <km-scale craters is indicated by their progressive underabundance at smaller sizes relative to Ganymede's dark terrain (cf. McKinnon and Parmentier 1986, Chapman *et al.* 1999, Bierhaus *et al.* 2000). The general drop-off in numbers of small craters may partly reflect a relative dearth of small cometary impactors (Chapman

et al. 1998). But differences between Ganymede and Callisto indicate strongly size-dependent crater destruction on Callisto, since the same impactors strike both moons. We associate size-dependent crater loss with the disaggregation process, which liberates materials that evidently fill in crater floors and form exterior bajadas beneath their crumbling ramparts.

There is a caveat to any generalizations about Callisto's geology: it was the least thoroughly imaged satellite by *Galileo*. Very high-resolution (15 m/pixel) images from orbit C21 reveal relatively more small craters on Callisto (Bierhaus *et al.* 2000, Wagner *et al.* 2000). Bierhaus *et al.* (2000) suggest that these small craters might be mainly secondaries from a recent impact. Wagner *et al.* (2000) interpret the majority not in clusters as primaries, which have thus not been erased by disaggregation. Eventually, studies of small craters on well-imaged Europa may resolve the issue by establishing the primary crater production function in the Jupiter system (eFigure 17.2).

Generally, Callisto's surface is either bright (geometric albedo ~0.8) or dark (~0.2) with little in between. Bright material, generally on or near the crests of high-standing topography, is probably frost (e.g., Spencer 1987a). Such frost deposits may be thin, less than a few meters; they certainly do not appear to change, mute, or exaggerate the topography or shape of these outcrops at >10 m scales. Large, bright expanses appear texturally rough, have steep, inconstant slopes, and otherwise look like unmantled bedrock (Figure 17.14). Large expanses of bright surfaces, such as the scarp seen in Figure 17.14, appear texturally rough, have steep inconstant slopes, and exhibit the overall appearance of an otherwise unmantled bedrock. The dark material at the base of scarps sometimes forms a smooth-textured lower component of constant-angle slope, as seen at the base of the scarp in the left side of the figure (see slopes between black arrows in Figure 17.14). The contact of the lower dark material with the rugged and steeper upper slope may trace out upward-pointing "V"s, implying that dark material has moved from upslope, perhaps down chutes (see slopes below white arrow in Figure 17.14). Of course, frost would be expected to form preferentially on high thermal inertia bedrock, which would remain colder throughout the day.

In contrast, dark material is almost always in low-lying areas, or in plains far from any relief. Below scarps, it may form a smooth-textured bajada with constant gradient (between black arrows, Figure 17.14). Contacts of the dark unit with rugged, steeper upper slopes form fan-like upward-pointing "V"s, implying that dark material was derived from upslope, possibly by moving down chutes (e.g., white arrow in Figure 17.14). The thermal inertia of dark material implies that it is composed of unconsolidated micron-sized particles. Appearing smooth in the highest resolution images, dark material forms patches up to 5 km across within crater floors or in intercrater depressions (Figure 17.15). Dark material could fall on Callisto from external sources, perhaps derived from Jupiter's small outer satellites (McKinnon and Parmentier 1986). However, regional color variations of dark material (Denk *et al.* 1998) suggest a crustal rather than exogenic source, consistent with its apparent local erosional derivation from bedrock-supported landforms such as crater rims.

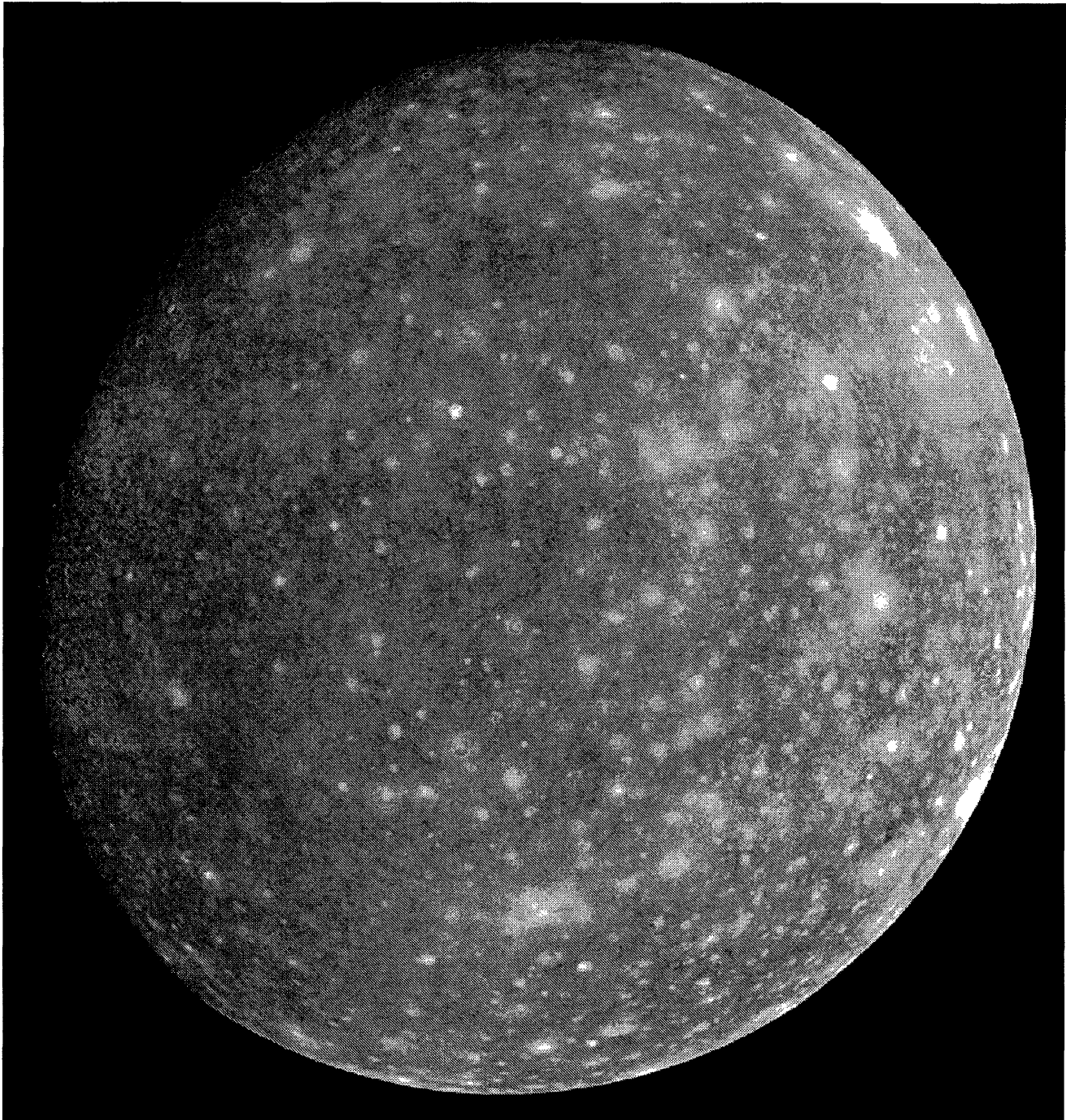


Figure 17.9. Global view of Callisto (~ 3 km/pixel). At this (typical for *Voyager*) resolution, only Callisto's ubiquitous impact cratering can be discerned, lending credence to its post-*Voyager* reputation as boring. The multi-ringed impact basin Asgard is seen along the limb at the 2 o'clock position. (Nine-image mosaic, centered at 17°N , 151°W , *Voyager 2* images FDS 20606.21, 25, 29, 33, 37, 41, 45, 49, and 53. The terminator is near the left limb. North is up. Callisto's diameter is 4818 km for scale.)

17.3.1 Large Scale Mass Wasting and Ground Collapse

Generally, large discrete mass wasting deposits like those on Callisto are not found on the other icy Galilean satellites, suggesting fundamental differences in crustal properties. Degradation on Callisto suggests either more effective surface processes responsible for slope destabilization or dif-

ferent surface layer properties (Moore *et al.* 1999, Chuang and Greeley 2000).

Kilometer-scale mass movements are sometimes accompanied by lateral spreading of the fallen material (Figure 17.16). Eleven deposits, 9°S – 28°N latitude, were investigated by Chuang and Greeley (2000), including those termed "debris aprons" by Moore *et al.* (1999). All lie within impact craters up to 28 km diameter and appear to be derived from

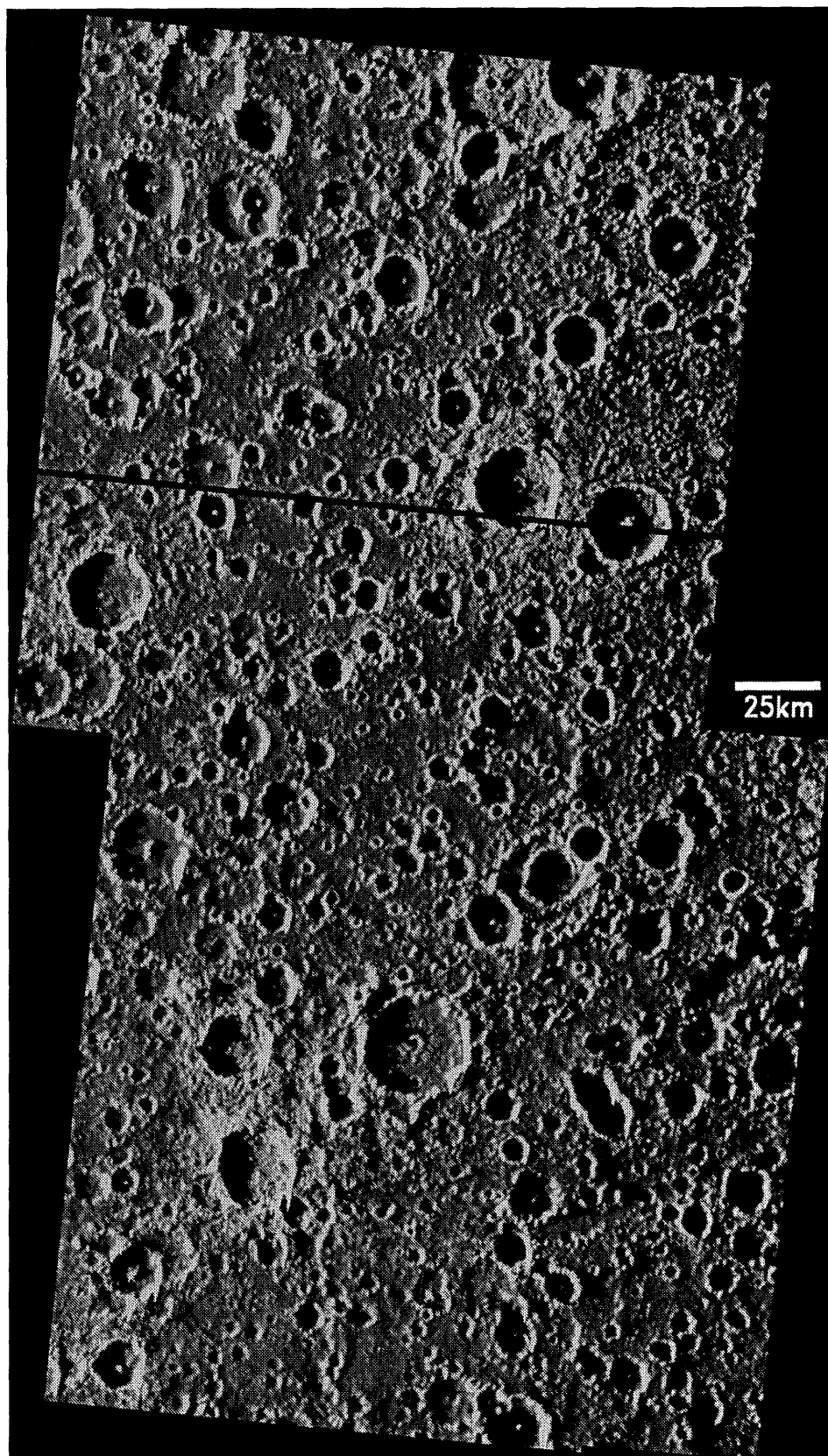


Figure 17.10. Moderate resolution (260 m/pixel) *Galileo* image taken near the terminator, showing representative cratered plains at 7° N, 183° W. Even though the resolution of these images is an order of magnitude better than those in Figure 17.19, the dominant geologic process expressed at this scale is still impact cratering. (*Galileo* frames PICNO 20C0010 and 11. North is up. Illumination is low and from the left.)

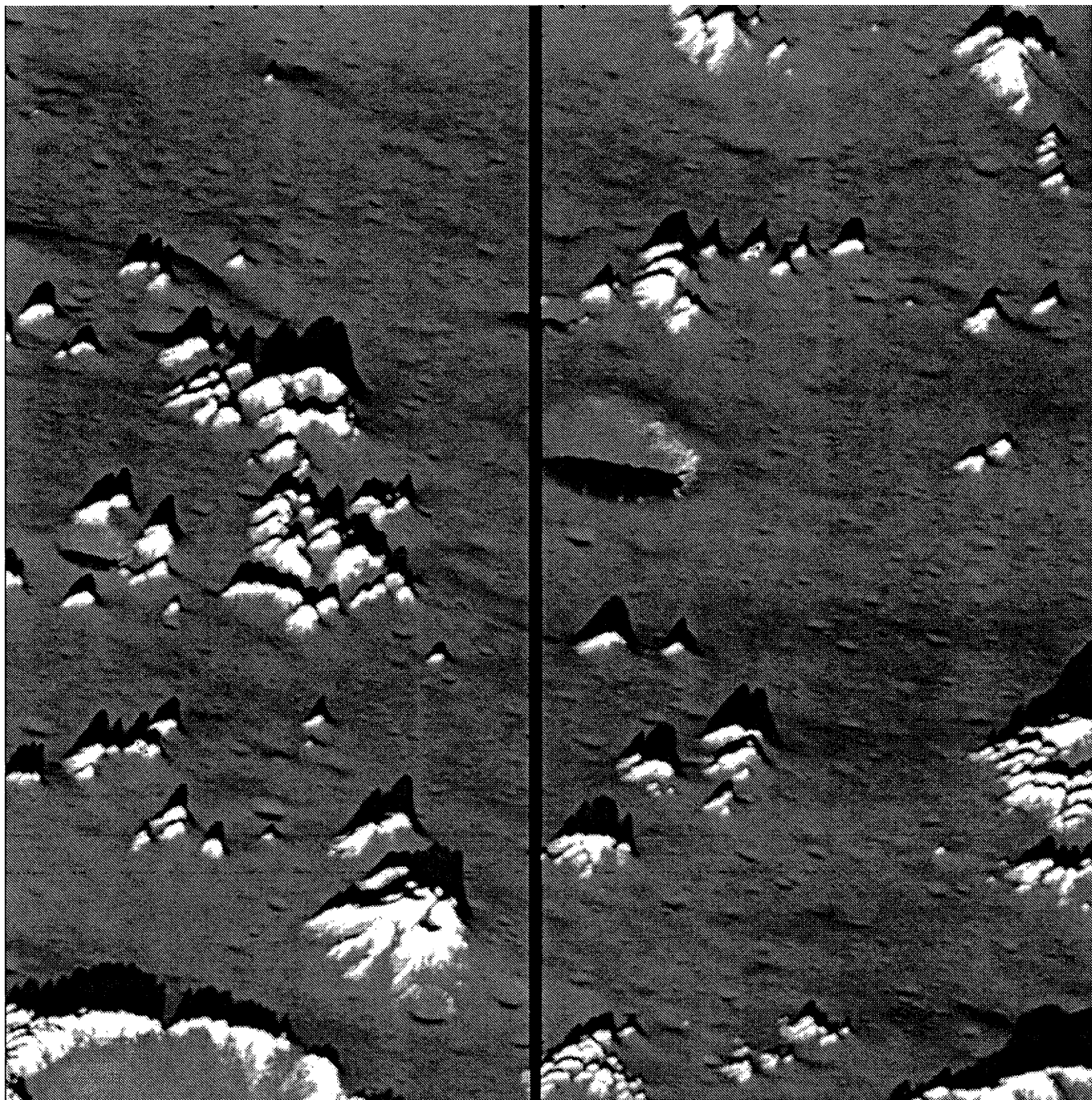


Figure 17.11. Very high resolution (~ 10 m/pixel left-right) oblique view of the surface of Callisto. At this scale it is apparent that the initially impact-sculpted surface has been subsequently massively eroded to form isolated knobs and dark low-lying fields of detritus. Bright frost coats local high points. (*Galileo* image PICNO 30C004, centered 12.30° N, 120.76° W. Image coverage is 7.9 km left-right and 14.1 km up-down. North is to the right. Illumination is low and from the bottom.)

crater walls. Similar aprons on other planets have been interpreted as debris avalanches (e.g., Sharpe 1939, Sharp 1973b, Malin 1992). Chuang and Greeley (2000) distinguish three morphological types: lobate, blocky, and slump-like. Most are lobate, with single, tongue-like lobes up to 9.9 km long (see Chuang and Greeley 2000, Table 2). Their margins are straight and their surfaces smooth, with no pits, grooves, or textures at the resolution limit (88 and 160 m/pixel). Volumes range 2.4×10^8 – 9.4×10^{10} m³, averaging ~ 90 m thick at frontal margins. Their morphology resembles terrestrial

rock glaciers interpreted to have deformed plastically, exhibiting Bingham rheology. If such rheology applies to Callisto, calculated lobate deposit yield strengths are comparable to those of terrestrial dry-rock avalanches, 9×10^2 – 3×10^4 Pa (Chuang and Greeley 2000). Although water-saturated debris flows have similar yield strengths, no cosmochemically reasonable liquid could lubricate materials on Callisto. Also near-surface bedrock temperatures are too low for ice to plastically deform, even over the age of the solar system (eFigure 17.3).

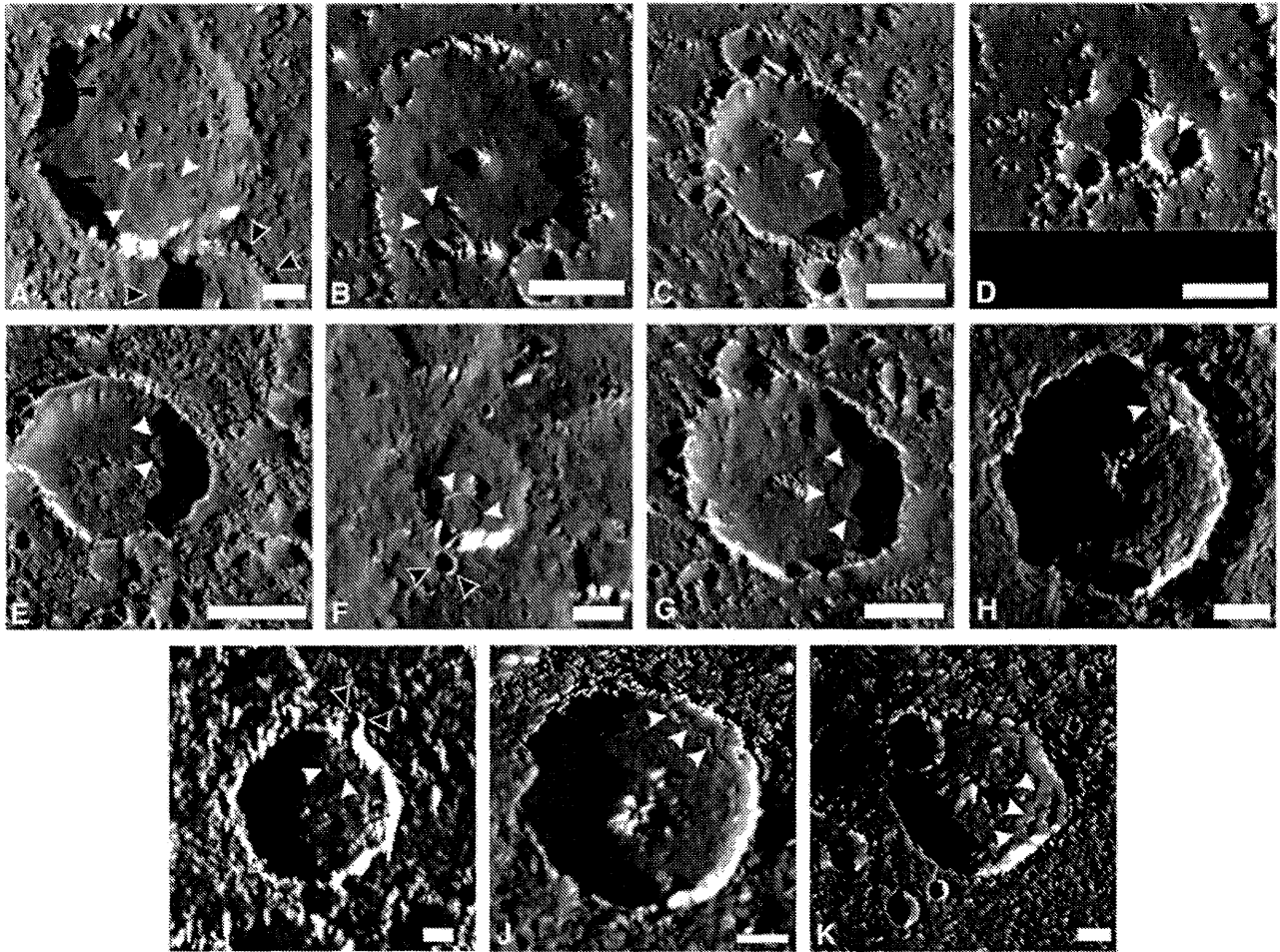


Figure 17.16. Individual mass movement deposits identified on Callisto with the following morphological types: lobate (a-i), blocky (j), and slump-like (k). White arrows point to the deposit. Black arrows outlined in white point to craters whose impact energy may have triggered the mass movement. The scale bar for all images is 5 km. North is to the top.

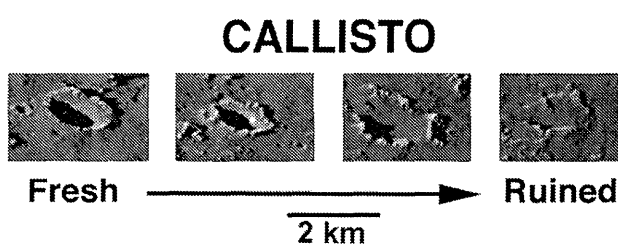


Figure 17.12. Kilometer-scale craters on Callisto range from those with more-or-less continuous, sharp-crested bright rims and bowl-like interior topography to craters with discontinuous rims and shallow interiors. These examples were all taken from low-sun, 50 m/pixel oblique images. Illumination is from the left. The left two examples are located near $\sim 38^\circ$ N, 35° W; the right two examples are near $\sim 35^\circ$ N, 46° W. (Excerpted from *Galileo* images PICNO C3C0044, 45, 65, 66.)

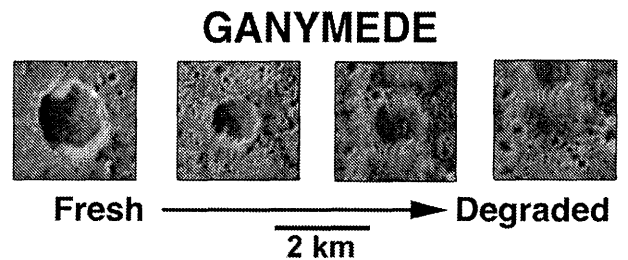


Figure 17.13. Kilometer-scale craters on Ganymede's dark terrain show a range of morphologies, which are generally characteristic of modification by the subsequent rain of mostly smaller impacts. These examples were all taken from low-sun, 21 m/pixel near-nadir-looking images. Illumination is from the left. North is up. The examples are located near $\sim 14^\circ$ S, 319° W. (Excerpted from *Galileo* images PICNO 28G0005, 8, and 9.)

Comparing the height versus length ratio (H/L) with slide volume suggests that Callisto's debris aprons are smaller and less energetic than most mass movements on the Moon, Mars, or Io (Figure 17.17a, Moore *et al.* 1999, based

on Bulmer 1994, and Schenk and Bulmer 1998). McEwen (1989) suggests that martian landslide emplacement has half the run-out efficiency typical of Earth, and the same may be true of Callisto, perhaps due to gravitational effects on

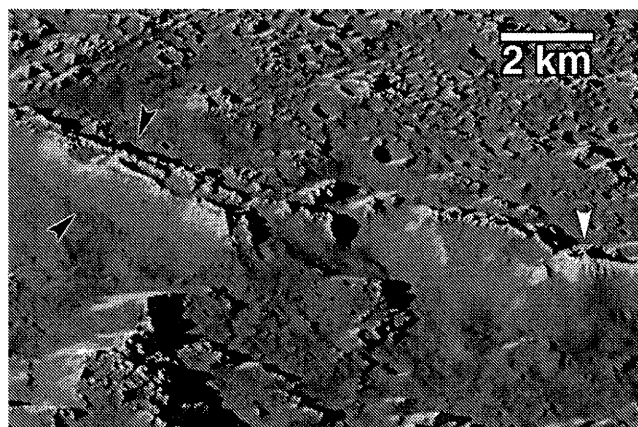


Figure 17.14. Bright and dark material on Callisto's surface seen at low sun and high resolution. Oblique, 40 m/pixel image of a part of the southern wall of Gomul Catena at 35° N, 46° W. Illumination is from the lower right. (A portion of *Galileo* image PICNO C3C0046.)

yield strengths (McEwen 1989) or lack of a lubricating inter-pore liquid or dense atmospheric gas (e.g., Brunsten 1979, p. 142). Alternatively, there may be differences in the type and amount of available loose material (e.g., Varnes 1958). In Figure 17.17b, H/L is plotted against run-out distance, including Venus escarpments (Malin 1992). Callisto's debris aprons plot among the shorter terrestrial run-out sub-aerial mass movements, despite their nonterrestrial inefficiency, which may account for their characteristic thickness and lobate margins.

Two mechanisms, undermining/oversteepening of slopes by sublimation erosion and seismic triggering, may work together to trigger mass movements on Callisto (Moore *et al.* 1999, Chuang and Greeley 2000). Chuang and Greeley (2000) propose a sequence starting with sublimation of primordial callistan crust, which forms a near-surface lag deposit proposed by Moore *et al.* (1999). Large impacts excavate down to the volatile-rich subsurface, exposing it to sublimation degradation, which then undermines the lag material causing it to fail, possibly triggered by seismic energy from a nearby impact. Several mass movements are near subsequent impact craters, but formation of large >100 km craters >200 km away could also have triggered landslides (Chuang and Greeley 2000). Creation of debris aprons may contribute to crater enlargement through scarp retreat (eFigure 17.3).

A 375 km × 225 km region at 1° S, 6° W (Figure 17.18) shows a landscape with numerous pits, which often occur in clusters (Moore *et al.* 1999). They are sharply outlined, closed depressions with steep walls but no raised rims. Outlines range from simple and smoothly curving to complexly convoluted, but are rarely angular; some pits coalesce or are barely separated from one another by septa. Pits have a mono-modal size distribution, peaking near 1 km but skewed toward smaller sizes (Merline *et al.* 1998); the largest ones are nearly 1 km deep. Pit configuration and morphology are inconsistent with a secondary impact origin; if they were initially secondary craters, they have been greatly modified. Resembling martian polar etched pits first described by Sharp (1973a), Callisto's pits may have formed from initially

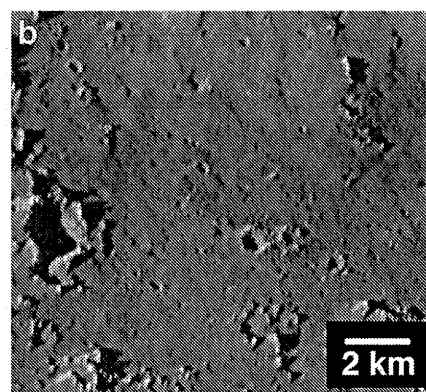
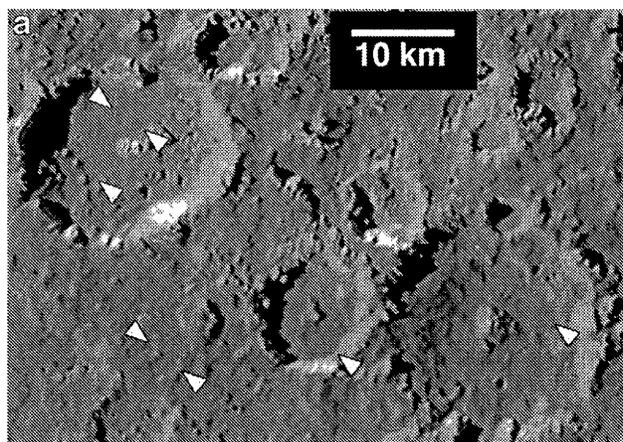


Figure 17.15. (a) Smooth patches (see arrows) of dark material on Callisto, approaching 5 km across, can be seen within crater floors or in intercrater depressions in this low-sun, 160 m/pixel image. The absence of topography within smooth patches implies that the dark material may be locally many meters thick. Scene center coordinates are ~38° N, 35° W. (A portion of *Galileo* image PICNO C9C0010.) (b) Dark material commonly appears smooth even in the highest resolution images. This low-sun (incidence angle ~85°), 37 m/pixel image shows a few several-hundred-meter-scale craters. Scene center coordinates are ~8° S, 7° W. In both images north is up and illumination is from the west. (A portion of *Galileo* image PICNO C3C0066 in orthographic projection.)

unremarkable local depressions by differential sublimation of a volumetrically substantial volatile. Solar energy is concentrated in the centers of growing pits, more efficiently with increasing size. At equatorial locations direct sunlight can penetrate even deep pits. The uneven distribution of pits and pit clusters may reflect a heterogeneous distribution of the responsible subsurface volatile.

Several crater walls are gullied with radial valley-like incisions (Moore *et al.* 1999) in N- or NE-facing crater walls. Individual "gullies" in Figure 17.18 are <500 m wide and <4 km long, extending from crater rim crests down to floor levels. Many other craters in the same scene show subtler radial patterns on parts of their walls. Since erosion by fluid drainage and downcutting is very unlikely, perhaps the same process that forms pits and predisposes debris avalanches is widening pre-existing fractures in and beyond the crater walls.

17.3.2 Knobs

By far the most common positive relief landform on Callisto are knobs, which appear to be remnants of crater rims, central peaks, and ejecta deposits (Moore *et al.* 1999, Basilevsky 2002). Basilevsky measured heights of 24 typical knobs seen at very low sun (incidence angle 81.6°) and high resolution (15 m/pixel) at 1° N, 106° W (Figure 17.19). Knob profiles (Figure 17.20) have simple conical shapes. Summits are usually rounded and slope-foot junctions are sharp with no gradual transition. Flank steepness varies $17\text{--}56^\circ$ with a mean of $31.4^\circ \pm 7.9^\circ$, which is roughly the angle of repose.

The evolution of initially continuous deposits into discrete knobs can be inferred by comparing ejecta and/or impact melts associated with fresh impact features on Ganymede with similar-sized degraded impact features on Callisto. Whereas impact craters on Ganymede often show continuous proximal ejecta deposits that gradationally blend with the surroundings, a similar-sized crater on Callisto is often surrounded by a field of knobs immediately beyond its rim (Figure 17.21). Larger impact features such as palimpsests show similar contrasts between the two satellites. Buto Facula, a penpalimpsest on Ganymede, exhibits deposits of melt and proximal ejecta with continuous undulating textures and a few imbedded blocks (eFigure 17.4), whereas a palimpsest on Callisto at $\sim 14^\circ$ N, 352° W, which appears smooth at *Voyager* resolutions, is seen by *Galileo* (eFigure 17.5) to consist of a field of closely spaced, small, bright-crested knobs, each a few hundred meters to ~ 1 km across (Figure 17.22). Presumably the callistan palimpsest originally resembled Buto Facula before degrading into a field of knobs. The non-knobby appearance of melt and ejecta associated with Lofn, a young palimpsest-like feature on Callisto, supports the assumption that palimpsests on Callisto initially resemble those on Ganymede.

17.3.3 Erosional Processes on Callisto

On the icy Galilean satellites, sputtering, impact-derived regolith production, and sublimation probably all play roles in the evolution and redistribution of their surficial layers.

Sputtering

The potential effect of sputtering decreases greatly with distance from Jupiter. The effectiveness of sputtering on ice is 20 times less at Ganymede and 100 times less at Callisto than at Europa (Johnson 1990). Shoemaker *et al.* (1982) point out that the ice-rich crater rays on Ganymede, which have survival ages of order 1 Gyr, are probably just a few meters thick and thus indicate that ice sputter-ablation rates on Ganymede may be less than a few meters per Gyr. Sputter ablation rates on Callisto are presumably lower and of very minor importance.

Impact Cratering and Regolith Generation

Callisto is covered by a pervasive, smooth, slightly undulating unit composed of generally homogeneous, low albedo material (Figure 17.15). Its visibility is enhanced by the paucity of small craters in many areas, which may be partly

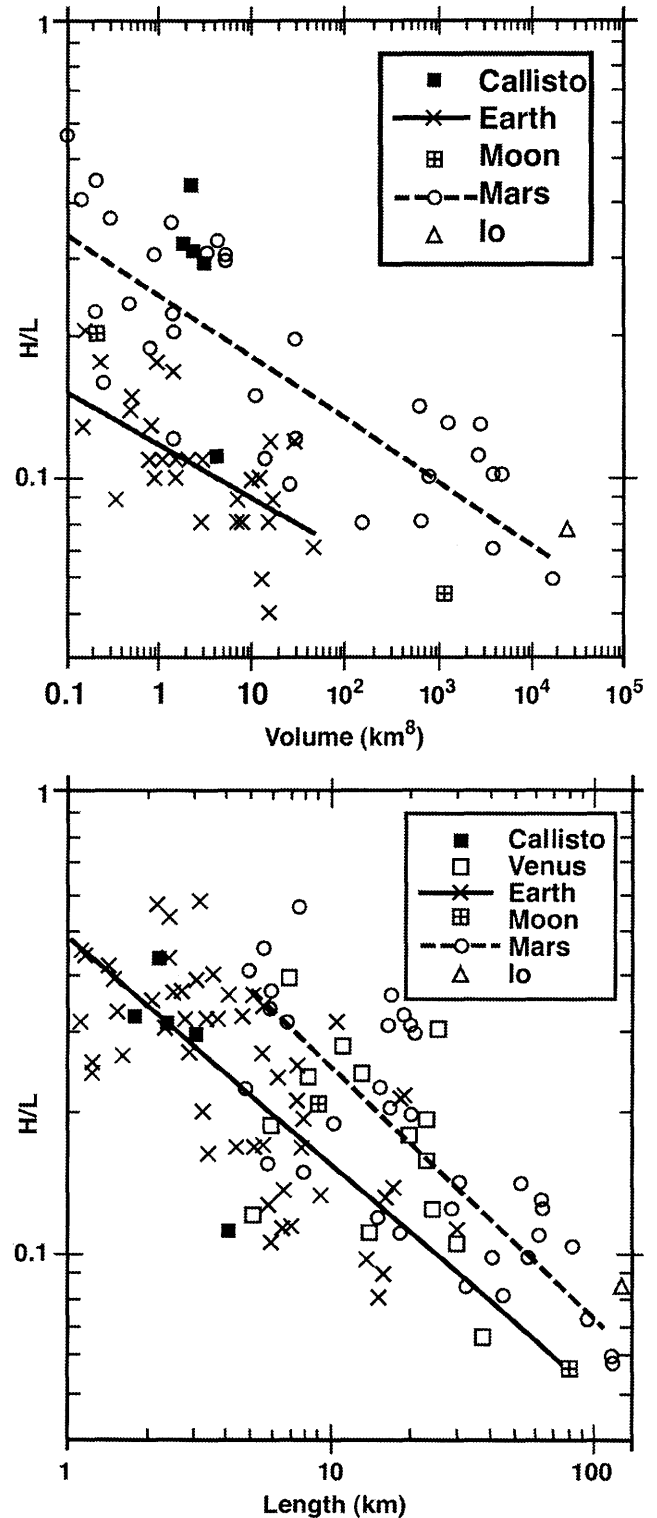


Figure 17.17. Plots of callistan debris aprons height-over-length ratios (H/L) versus (a) volume and (b) run-out length, along with a field of measurements for similar mass movements on other objects. Non-Callisto data taken from Bulmer (1994), Schenk and Bulmer (1998) and Malin (1992).

attributable to a lower ratio of small-to-large impacting projectiles in the Jupiter system compared with the inner solar system (Chapman *et al.* 1998). Nevertheless, the spectrum of morphologies of small craters demonstrates that there is an ongoing process of small-crater degradation.

On other familiar, inner solar system bodies, small crater degradation is often due to the continual erosion by smaller-scale impacts and redistribution of ejecta, due to an impactor size distribution characterized by a large (“steep”) negative power-law exponent. This process is well illustrated on the lunar surface at spatial scales smaller than a few hundred meters (e.g., Soderblom 1970, Chapman *et al.* 1996). But such lunar-like processes are manifestly not at work on Callisto, since its population of small impact craters is an order of magnitude below the “saturation equilibrium” density maintained (for “steep” impactor size distributions) by the competing formation and degradation/destruction of craters by the impact process alone, and even farther below the higher equilibrium density for the shallower production function that may apply to the Jupiter system. From experiments (Gault 1970), numerical simulations, and direct observation of planetary surfaces, the nature of saturation equilibrium is well understood (e.g., Chapman and McKinnon 1986). In principle, Callisto’s low small-crater densities could be maintained by a sandblasting process due to an even larger power-law exponent, but such steep power laws have not been identified for any equilibrium population of interplanetary debris. The possibility that the smooth unit could have been emplaced by ejecta blanketing from the formation of the abundant larger craters and basins on Callisto is ruled out by the spectrum of small-crater morphologies and by comparison with equivalent attributes of the Moon, where such a unit is not manifest. Therefore, some other process besides impact generated and redistributed regolith must be responsible for the smooth plains of Callisto (Moore *et al.* 1999).

Sublimation Degradation

The degradation of small craters is probably related to the deposition or creation of the plains unit itself (Moore *et al.* 1999). Sublimation degradation has been proposed as an agent of km-scale landform modification on several Galilean satellites (McCauley *et al.* 1979, Moore *et al.* 1996, Moore *et al.* 1999, Chuang and Greeley 2000). Sublimation processes relevant to (non-comet) icy bodies have been modeled by several researchers (Lebofsky 1975, Purves and Pilcher 1980, Squyres 1980, Spencer 1987a, Colwell *et al.* 1990, Moore *et al.* 1996). Purves and Pilcher (1980) and Squyres (1980) both concluded that Ganymede and Callisto should accumulate frost at their poles at the expense of the equatorial regions where exposed ice should entirely sublimate away. Spencer (1987a) modeled the thermal segregation of H₂O ice on Ganymede and Callisto and concluded that sublimation is the most significant process for the redistribution of ice at sub-kilometer scales. Pole-facing slopes are often brighter than equator-facing slopes, suggesting sublimation from the latter, resulting in a refractory-rich lag deposit, and precipitation of frost on the poleward slopes (Spencer and Maloney 1984, Prockter *et al.* 1998a).

Topographic thermal models for airless bodies (e.g., Winter and Krupp 1971, Spencer 1990, Colwell *et al.* 1990)

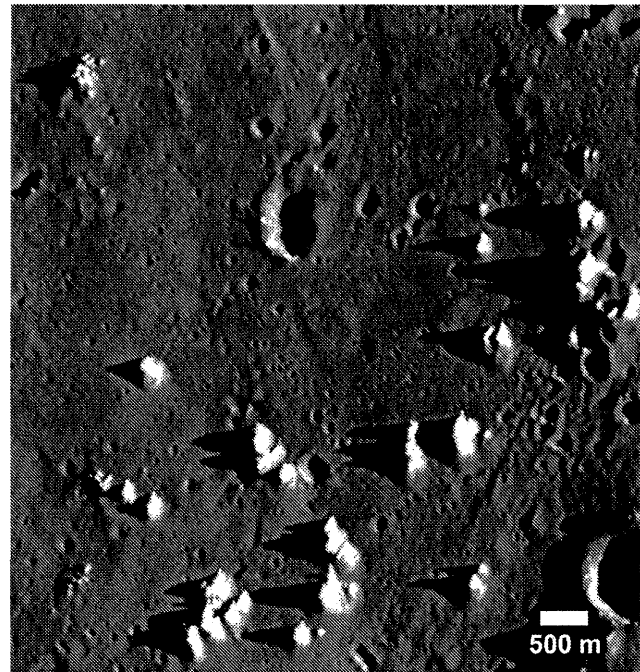


Figure 17.19. Very high resolution (15 m/pixel) near-nadir view of typical knobs on Callisto. Note the very short top-of-frame-pointing bright image artifacts caused by pixel saturation and CCD bleed from overexposed very bright frost deposits on the summits of the knobs. The fortuitous lighting and geometry of this scene nevertheless permits the profiles of knobs to be derived from their shadows. (A portion of *Galileo* image PICNO 21C0004, centered 0.94° N, 106.56° W. North is up. Sun is low and from the right.)

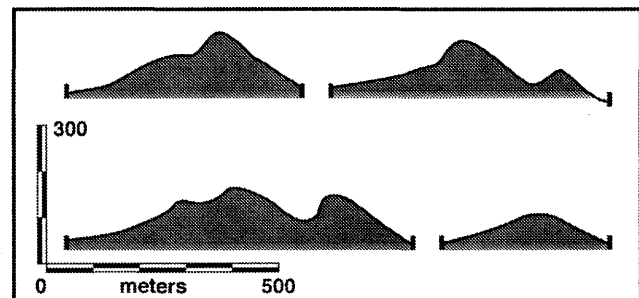


Figure 17.20. Examples of profiles of knobs, some of which are seen in Figure 17.19 (modified from Basilevsky 2002).

consider scattering and re-radiation of reflected and thermal radiation from various topographic elements, including diurnal subsurface heating variations. They show that high-latitude, poleward-facing slopes are cooler than average surfaces and are natural sites for accumulating frost deposits (Spencer and Maloney 1984) (Figure 17.23.). At low latitudes, temperatures are higher in depressions, because depressed surfaces receive thermal and reflected solar radiation from their surroundings. Low-latitude depressions, therefore, are expected to be sites of net sublimation of initially icy surfaces and should develop lag deposits somewhat faster than plains surfaces of the same albedo (Figure 17.24). Therefore, bright, icy interior crater walls at low latitudes, commonly seen on Callisto, require additional explanation.

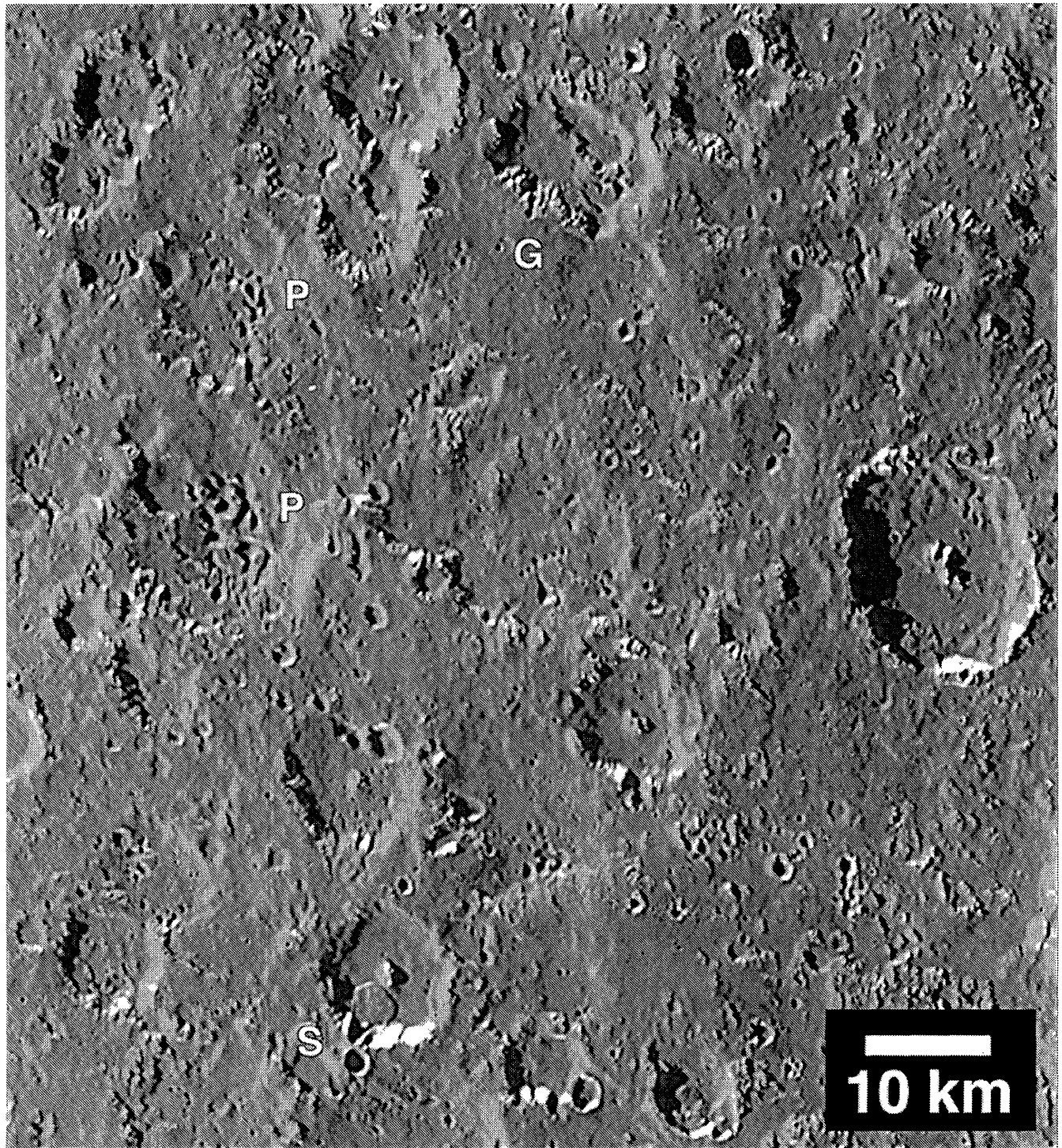


Figure 17.18. Irregularly-shaped pits (see near P), “gullies” (see near G), and a debris apron (see near S) all observed in this 160 m/pixel resolution image of equatorial Callisto. North is up and illumination is low and from the west. Scene center coordinates are $\sim 6^\circ$ S, 7.5° W. (A portion of *Galileo* image PICNO C9C0007.)

Possibly, lag deposits are sloughed off these steep slopes by gravity, exposing outcrops of dark, dirty-ice, high thermal inertia bedrock, which act as cold traps and become even colder once frost forms.

The other preferred site for bright, low-latitude deposits is on the sides and summits of the numerous, isolated knobs. Sloughing of lag deposits and re-frosting of bedrock might

explain the bright slopes of knobs, but their bright summits are problematic. Quantitative thermal modeling of positive relief features is more difficult than for craters, whose interior temperatures are influenced only by other parts of the crater; hill temperatures are influenced by, and affect, wide surrounding areas. Semi-quantitative modeling by Moore *et al.* (1999) yields some insights (see Appendix A on the

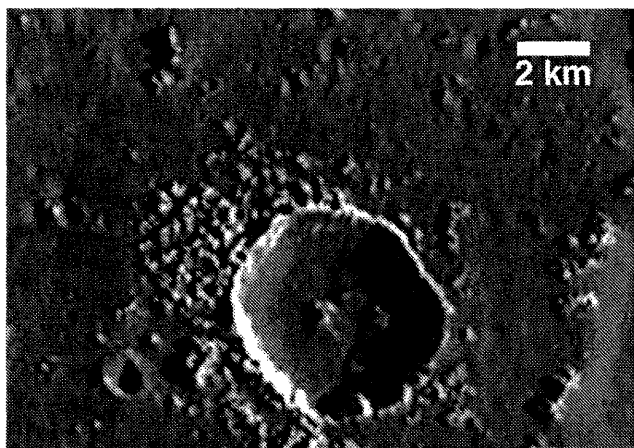


Figure 17.21. Example of ejecta around ~5 km crater, illustrating the effects of knob-forming erosion on Callisto. (Portion of *Galileo* image PICNO 10C0012 centered ~14° N, 142° W. North is up and the Sun is low and from the right.)

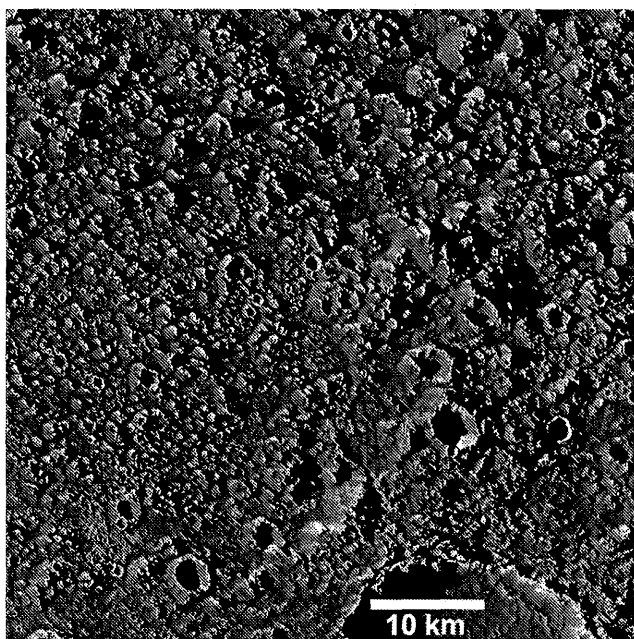


Figure 17.22. *Galileo* image of a palimpsest, imaged at 71 m/pixel showing abundant small erosion-formed knobs and a paucity of small impact craters. This material is mapped as “smooth plains” because of its appearance at km-scale resolutions from which the initial global geologic maps were derived. (*Galileo* image PICNO 10C0020, centered ~14.23° N, 350.81° W, North is up. Sun is low and from the left.)

accompanying CD). They concluded that the widespread degradation of Callisto’s landforms implies that CO₂ is a significant component (a few tens of percent) of the relief-supporting ices in the upper crust as other candidate materials are too refractory (Figure 17.25).

17.3.4 Putative Tectonic Features

Callisto does not appear to be tectonically active. Nonetheless, potentially tectonic features have been identified in a

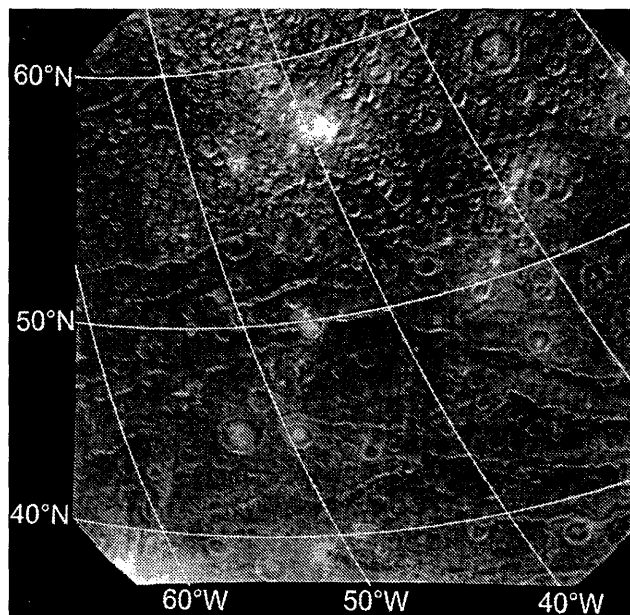


Figure 17.23. High latitude region of Callisto north of the Valhalla multi-ringed impact feature, showing bright patches on north-facing (pole-facing) crater walls. The true illumination direction is from below. For scale, the distance between 10° of latitude is ~420 km. Portion of *Voyager 1* image, FDS 16424.48.

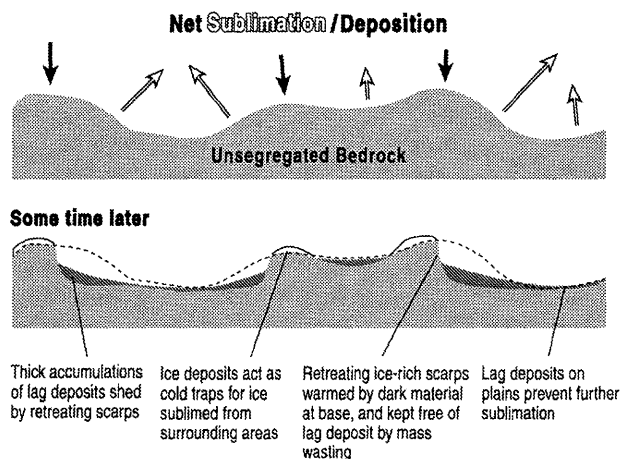


Figure 17.24. Net volatile sublimation/deposition surface evolution diagram. See text.

few areas. Lineaments in *Voyager* images of Callisto were identified by Wagner and Neukum (1991, 1994) and by Schenk (1995). Some are tentatively interpreted as extensional, and resemble the older system of narrow grooves oriented at high angles to the main furrow system of *Galileo* Regio on Ganymede (e.g., Schenk and McKinnon 1987, Murchie *et al.* 1990). At least five sites with lineaments have been identified (8° S, 255° W; 29° N, 256° W; 55° N, 340° W; 0°, 353° W; 43° N, 358° W). Thomas and Masson (1985) mapped scarps, furrows and lineaments in the Valhalla basin. Apart from concentric or radial scarps or furrows, they noted NW–SE- and NE–SW-oriented lineament directions. These directions are somewhat different from the NNW–SSE and ENE–WSW-oriented lineaments reported

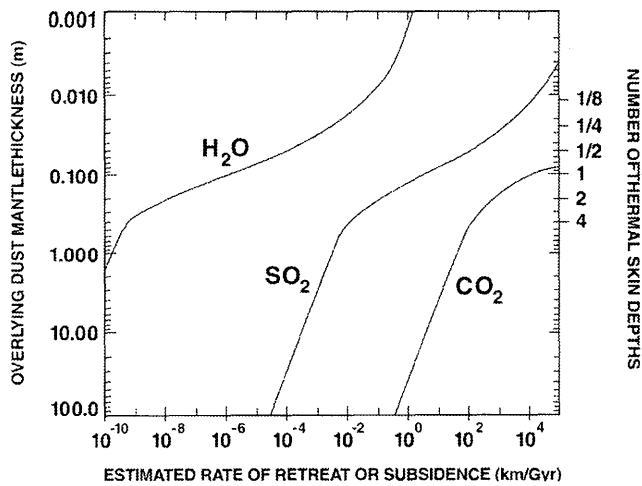


Figure 17.25. Sublimation rates of different volatiles on Callisto as a function of overlying lag thickness. The lag is modeled as a fine grain, low thermal inertia particulate. See text.

by Wagner and Neukum (1994) in the area east of Valhalla. The occurrence, ages and dimensions of all of these lineaments, if real (such fabric was not specifically targeted by *Galileo*), could provide important clues to Callisto's thermal history and possible early global expansion. An early period of tidal despinning might form a pattern of equatorial and mid-latitude strike-slip faults oriented in the sense mapped by Thomas and Masson (1985), but they would have been obliterated by subsequent cratering bombardment unless reactivated. The various orientations predicted by Melosh (1977) for a tidally despun body are not generally verified so far on Callisto. The possibility that these features are poorly resolved knobs unrelated to tectonism remains.

Schenk (1995) found an unusually large system of at least 10 radially oriented, double-walled grooves very near Callisto's north pole (Figure 17.26, eFigure 17.6). They are continuous over several hundred kilometers, average 2–4 km in width, and are relatively young as they cut across all craters in their paths. The longest extends ~800 km from the estimated center of the system, 79° N, 280° W. Endogenic and impact origins for this radial system have been evaluated (Schenk 1995), but no satisfactory images of the system's center exist to confirm an interpretation. Radial fracture patterns are observed around some large craters on Ganymede (e.g., Asphaug *et al.* 1998, Prockter *et al.* 1998b) as well as Callisto itself, suggesting an impact induced control of the tectonic pattern for the polar features.

Large Impact Feature Morphology and Related Landforms

Pristine impact craters are rare due to pervasive degradation, but the youngest craters on Callisto are roughly comparable in shape and morphology to those on Ganymede (Schenk 1991, 1993, 2002, Chapter 16). For example, the simple-to-complex transition is ~2.6 km, similar to Ganymede, and depths of complex craters 2–26 km diameter are also indistinguishable (Schenk 2002). Chapter 18 discusses crater morphologies and histories, as well as surface ages from crater statistics for the icy Galilean satellites, including Callisto.

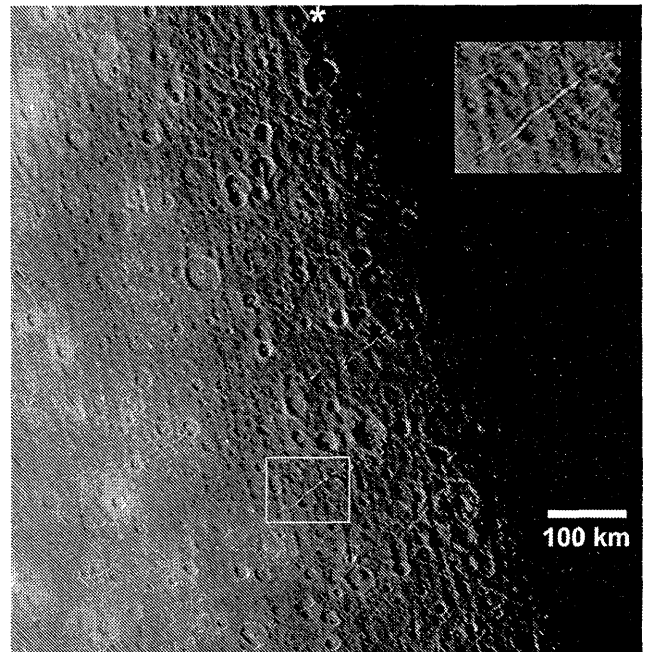


Figure 17.26. Radial groove system located near the north pole (star). Inset shows detail on groove. Grooves are interpreted to be tectonic. (Portion of *Voyager 1* image FDS 16426.46 centered ~88° N, 322° W, illumination is low and from the left.)

Doh, Lofn and Dome Craters

Several complex impact crater morphologies are seen in high resolution *Galileo* images. Especially interesting is the dome crater Doh (Figure 17.27), located near the center of the Asgard multi-ring basin. It is dominated by a large, smooth, but fractured dome ~25 km across, surrounded by a ~65 km wide ring of massifs. The rim itself is associated with a partially preserved outward-facing scarp at an effective diameter D of ~110 km. The rim of Doh (and similar craters), defined by easily mapped secondary craters, is located by scaling from the maximum extent of continuous ejecta (Schenk and Ridolfi 2002). Doh is an “anomalous dome crater”. These are similar to central dome craters (e.g., Osiris on Ganymede), but are noteworthy for lacking rim structures or relief; why, is unclear, but such intermediate-age dome craters on Ganymede may reflect an unusual period in Ganymede's thermal history. Counts of craters superimposed on Doh indicate that it is younger than Valhalla (Wagner *et al.* 1999).

The unusual Lofn feature (Figure 17.28) is an irregular bright patch in *Voyager* images (Schenk 1995), but is actually a complex impact structure (Greeley *et al.* 2000, Greeley *et al.* 2001). A central smooth region ~100 km across is surrounded by a crazed, fissured zone with an outer diameter of ~250 km, corresponding roughly with the bright patch. The surrounding pre-impact surface textures are smoothed out to $D \sim 725$ km. A complex concentric/radial albedo pattern extends out $D \sim 2000$ km. Greeley *et al.* (2001) equate the central smooth region with the crater floor and place the rim in the middle of the crazed zone. Using secondaries and ejecta–rim scaling, Schenk and Ridolfi (2002) show that the nominal rim location probably lies outside the rugged zone, at $D \sim 355$ km, making Lofn Callisto's

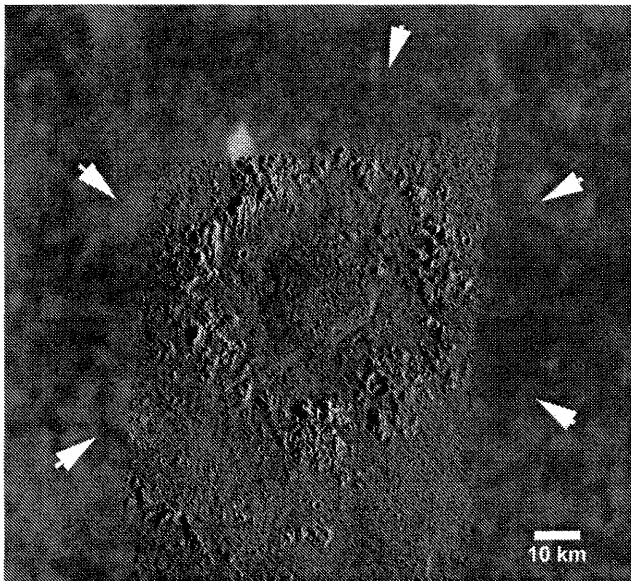


Figure 17.27. Doh, a morphologically fresh dome crater on Callisto. Arrows show location of the “crater rim,” which has a diameter of ~ 110 km. (Mosaic of *Galileo* images PICNO 10C0001 and 2, centered $\sim 31^\circ$ N, 142° W. North is up. Sun is low and from the right. Lower resolution *Galileo* image PICNO C3C0022 used for background.)

largest non-multi-ring impact structure. Crater frequencies place Lofn stratigraphically as post-Valhalla in age (Wagner *et al.* 1998, 1999), and possibly as young 2 Gyr (Chapter 18).

Lofn is apparently an anomalous dome crater like Doh, but much larger. The smooth and concentric rugged zones are structurally equivalent to the central dome and massif ring in smaller craters. The crater rim is not structurally expressed at Lofn, nor in anomalous dome craters generally (except perhaps for one or more concentric scalloped scarps in the NW quadrant near the nominal rim location). Lofn’s true depth is unknown, for lack of stereo images, and it has no rim (Greeley *et al.* (2001) report relief for part of the inner ring, not the rim). The morphology of Lofn and other anomalous dome craters suggests impact into an interior that is progressively weaker with depth and thus unable to support the topographic loads of large transient craters (Schenk 2002).

Multi-ring Impact Features

As reviewed by McKinnon and Melosh (1980), Merrill and Schultz (1981), Spudis (1993), and Greeley *et al.* (2000), multi-ring structures provide insight concerning target structure at the time of impact (Melosh 1989). Schenk (1995) classified various large impact features on Callisto as multi-ring structures, palimpsests, and “cryptic” ring structures. Seven multi-ring structures were identified on Callisto in *Voyager* images (Bender *et al.* 1997a); moderate resolution (0.4–1.1 km/pixel) *Galileo* images show some of them in more detail (Greeley *et al.* 2000) and include Valhalla, Asgard, Adlinda, Heimdall, and Utgard. Most are typified by a central zone, a higher-albedo zone covering and extending beyond the central zone, and one or more zones of concentric lineaments (e.g., scarps and troughs).

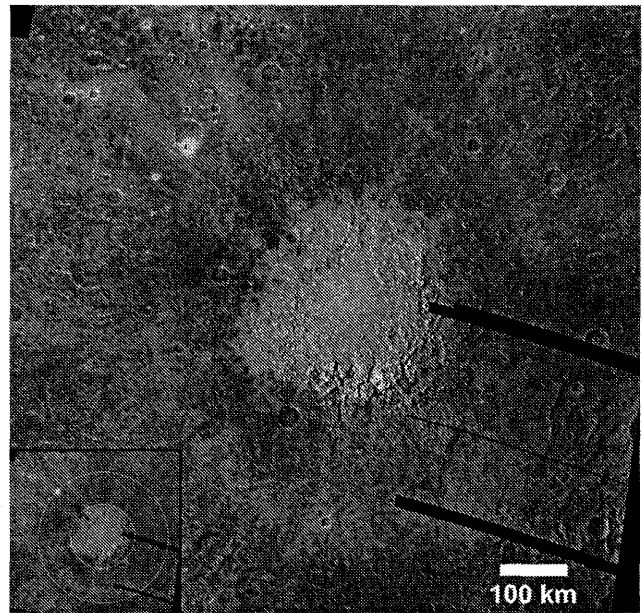


Figure 17.28. Lofn, a morphologically fresh large impact feature on Callisto. Inset shows the mapped onset of secondary craters (outer circle, diameter 725 km) and inferred location of the “crater rim” (inner circle, diameter 355 km) as derived from a scaling relationship developed by Schenk and Ridolfi (2002). (Mosaic of *Galileo* images from observation G8CSADLND01 projected to a feature-centered orthographic projection, centered $\sim 54^\circ$ S, 24° W. North is up. Sun is low and from the left.)

Valhalla. Valhalla (McKinnon and Melosh 1980, Schenk 1995, Greeley *et al.* 2000) has three prominent zones, a rather smooth central region, an inner ridge and trough zone, and an outer trough zone with $D \sim 3800$ km (Schenk, 1995), for which representative terrains were imaged by *Galileo* at 410 m/pixel (Bender *et al.* 1997b, Homan *et al.* 1997, Greeley *et al.* 2000). The central zone is ~ 360 km across, has a mottled, generally bright appearance, and is moderately cratered (Figure 17.29). Several dark-halo craters could reflect penetration into a darker substrate through a lighter layer < 1 km thick (McKinnon and Parmentier 1986). In a ~ 35 m/pixel frame (Figure 17.30), craters just a few hundred meters across are sprinkled among larger remnants of degraded crater rims and small knobs, all set in a background of smooth, low-albedo plains.

The inner ridge and trough zone extends out to $D \sim 1900$ km (Schenk 1995) and has asymmetric, degraded scarps/ridges with steep flanks facing outward from the structure. Many appeared to be continuous features in *Voyager* images but are really a discontinuous series of high albedo knobs. Troughs in this zone, as long as several hundred kilometers and up to 20 km wide, are slightly sinuous and appear to be grabens (Greeley *et al.* 2000). These ridges have relief of 2–3 km (Schenk *et al.* 1997).

The outer trough zone has an effective outer diameter of 3000 to 3800 km (depending on quadrant) and has double-walled, sinuous lineaments, probably grabens resulting from lithospheric extension (McKinnon and Melosh 1980, Schenk 1995). Moderate resolution *Galileo* images of the eastern trough zone (Figure 17.29) show irregular, discontinuous scarps comprising the trough. In some cases, older impact



Figure 17.29. Mosaic of *Galileo* images (outlined) taken at 410 m/pixel on orbit C9, set in a background of *Voyager* coverage, showing part of the Valhalla multi-ringed structure, centered at 15° N, 56° W, from its central bright zone (left side), the inner ring zone, and to the outer graben zone. Insets show locations of high resolution images in Figures 17.30 and 17.31. (Mosaic of *Galileo* images from observation C9CSVALHAL01 projected to a feature-centered Lambertian equal-area projection. North is up. Sun is from the left.)

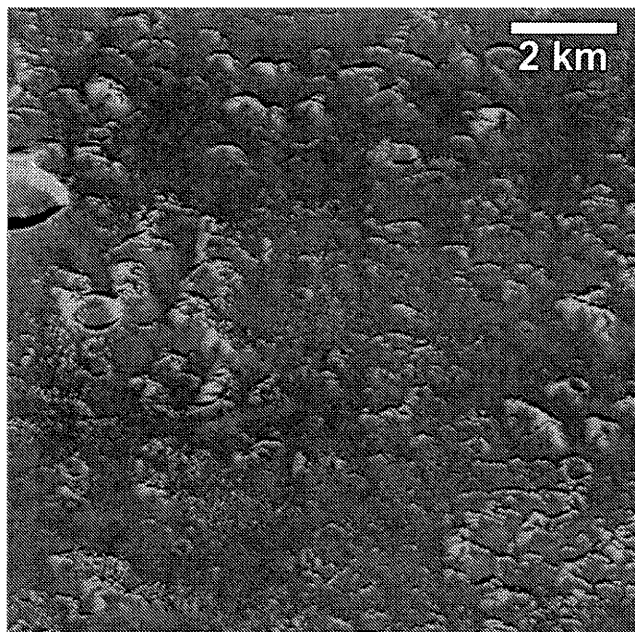


Figure 17.30. High resolution (~ 35 m/pixel) oblique *Galileo* image of the central zone of the Valhalla multi-ring structure showing bright knobs as large as a few hundred meters across, degraded impact craters, and low albedo smooth plains which tend to lack small craters. (*Galileo* image PICNO C3C0030, centered $\sim 15.31^\circ$ N, 54.56° W. North is to the left. Sun is low and from the bottom of the frame.)

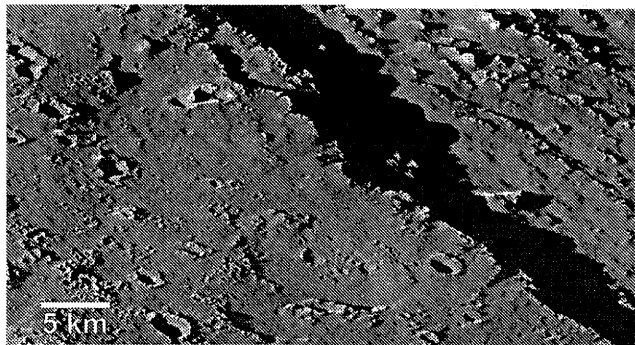


Figure 17.31. High resolution (~ 50 m/pixel) oblique mosaic of *Galileo* images showing the western scarp of a sinuous ring-tectonic trough associated with the Valhalla multi-ring structure. (*Galileo* images PICNOs C3C0065 and 66, centered $\sim 34.00^\circ$ N, 37.60° W. North is up. Sun is low and from the left.)

craters appear to control trough width and sinuosity (Klemaszewski *et al.* 1997); they may have weakened the lithosphere locally and influenced the development, location, and orientation of the troughs during and following the formation of Valhalla. Scarps in the outer trough region include both a prominent fracture and a series of parallel smaller scarps (Figure 17.31); evidently the graben failure zone extended over >30 km (Greeley *et al.* 2000). The “plains” flanking the trough include degraded crater rims and numerous small knobs. Despite post-*Voyager* suggestions of possible endogenic (i.e., volcanic) resurfacing in these regions (e.g., McKinnon and Melosh 1980, Remsberg 1981), *Galileo* images show no indications of flows (Greeley *et al.* 2000).

Valhalla lacks a clearly definable rim, but obvious secondaries exist at $D \sim 1800$ km, just beyond the edge of the inner ridge and trough zone, placing Valhalla’s nominal rim at $D \sim 990$ km, making it the largest known impact feature in the jovian system. Destruction of pre-existing craters and textures in the inner graben zone were thus probably caused by ejecta.

Valhalla Impact Antipode. A *Galileo* imaging target during the C30 flyby was the antipode of the Valhalla structure (15° S, 236° W) (Figure 17.32). Hilly, lineated, disrupted terrains exist in antipodal regions of other large impact basins (e.g., Mercury’s Caloris basin) due to propagation of impact-induced seismic waves. However, modeling by Watts *et al.* (1989) suggested that such disruption should not have occurred from the Valhalla impact. They found that, depending on impactor size and the nature of Callisto’s interior, the impact probably had insufficient energy to disrupt terrain at Valhalla’s antipode, given that a hypothesized liquid water layer in Callisto’s mantle should reduce antipodal pressures. Consistent with Watts *et al.*’s hypothesis, no disruption is evident in the 340 m/pixel *Galileo* image (Figure 17.32). More conclusive evidence for a liquid water layer within Callisto was obtained by the *Galileo* magnetometer (Khurana *et al.* 1998, Kivelson *et al.* 1999).

Asgard. Asgard (e Figures 17.7 and 17.8) consists of central plains surrounded by discontinuous, concentric scarps and an outer zone with sinuous troughs. The central bright unit is ~ 200 km across. Its high albedo is enhanced by the more recent crater, Doh, which apparently excavated icier (brighter) subsurface materials (Bender *et al.* 1997a). The central zone is partly enclosed by an inner zone of discontinuous scarps and massifs as wide as 8 km and up to 2 km high (Greeley *et al.* 2000). The asymmetric scarps face inwards, possibly due to lithospheric uplift at the time of impact. Most terrain between the inner scarp zone and the outer trough zone is moderately cratered and knobby. Ejecta deposits and secondary craters are missing around superposed impact craters, and craters <1 km diameter are scarce on the plains surrounding the knobs. Low albedo smooth plains, adjacent to some massifs and concentrically arrayed between the scarps and the trough zone, appear to embay older terrain, including small knobs and craters. However, no flow fronts or other indications of cryovolcanic activity are seen (Greeley *et al.* 2000).

Troughs in the outer zone, like those at Valhalla, are sinuous, discontinuous, and inferred to be grabens. The area beyond the southernmost trough lacks the usual knobby traits and has more superposed impact craters (Schenk 1995). The outer zone has a lower albedo than the surrounding cratered plains (Klemaszewski *et al.* 1998b), probably representing the extent of continuous ejecta; it has a diameter of 1250 km, for a nominal crater rim diameter of 670 km (Schenk and Ridolfi 2002).

Adlinda. Most of the Adlinda structure was imaged by *Galileo* at 876 m/pixel, so only its larger features can be studied (eFigure 17.9). Moreover, the ejecta from adjacent Lofn obscures $\sim 30\%$ of the structure. It is defined by sets of concentric lineaments and troughs, especially a nearly continuous, slightly sinuous trough ~ 520 km long to the southwest at an effective diameter of ~ 850 km. Shorter troughs are in a concentric band toward Adlinda’s center; both the long and shorter troughs appear to be grabens (Greeley *et*

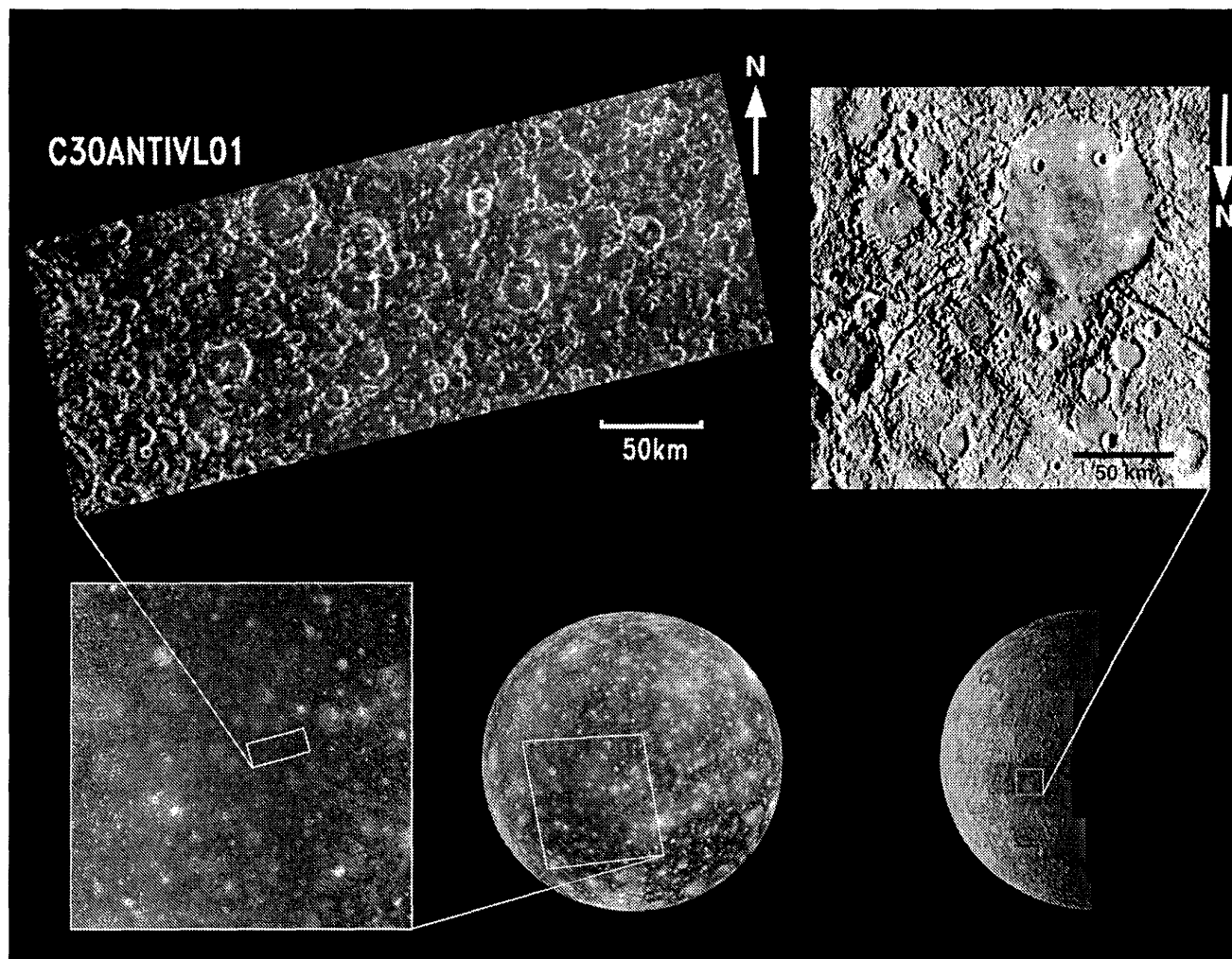


Figure 17.32. *Galileo* obtained a regional (340 m/pixel) observation (C30ANTIVL01) of a portion of Valhalla's antipodal region under high-sun illumination (*Galileo* image PICNO 30C0022, centered $\sim 13.8^\circ$ S, 229.9° W. North is up.). For comparison with the antipodal regions of Valhalla, the Caloris Basin antipole on Mercury is shown at a similar scale. In contrast to the mercurian scene, the image of the Valhalla antipode region shows no sign of disrupted terrain.

al. 2000). Adlinda's outer margin is defined by a contact, 20–40 km beyond the long trough, which encloses a low albedo band (Wagner *et al.* 1997) that embays surrounding cratered plains. This contact is inferred to be the extent of the continuous ejecta inside, which crater frequencies are significantly lower. Adlinda's northern side is defined by a series of lineaments of unidentifiable nature.

Possible Multi-ring Impact Features. Utgard (apparent diameter ~ 700 km) may be a multi-ring structure superposed on the northern side of Asgard (Greeley *et al.* 2000). Much of it is obscured by deposits from the impact crater Burr. It is defined by a concentric band of lineaments forming a ring about 610 km across, which, in turn, is surrounded by a slightly darker zone that might represent part of the ejecta.

Heimdall (eFigure 17.9), suspected in *Voyager* images, was subsequently imaged by *Galileo*. The western rim zone is very rugged and includes massifs 1 km high. Inner and outer bands of massifs are at $D \sim 220$ km and ~ 400 km, respectively. Bright ejecta rays can be traced more than 1100 km to the NE. Encircling structural lineaments are not obvious

around Heimdall, so it might be a large impact crater similar to its neighbor, Lofn. A single global *Galileo* image of a part of the trailing and sub-jovian hemispheres, showing Lofn and Heimdall, was taken during the late I31 orbit. Preliminary crater size–frequency data (R. Wagner, personal communication 2002) suggest a Valhalla/post-Valhalla, but pre-Lofn age, confirming stratigraphic indications, which may or may not be compatible with the possibility that Heimdall and Lofn represent a double impact.

Additional candidate multi-ring structures have been identified on Callisto by mapping sets of discontinuous, arcuate features (Greeley *et al.* 2000). For example, low albedo troughs imaged at 32° S, 66.5° W during the G8 orbit resemble the outer rings of Asgard and Adlinda (Klemaszewski 1998a), forming discontinuous concentric patterns that encircle higher albedo zones, which are interpreted as central plains units of degraded multi-ring structures. If considered as giant impact craters, such candidate features would imply a greater frequency of large impactors in the jovian sys-

tem than previously suggested by Chapman and McKinnon (1986).

17.3.5 Stratigraphy and Geologic Mapping

Callisto is relatively simple in terms of geological mapping at the global scale because there are so few distinct units (Bender *et al.* 1997a, Greeley *et al.* 2000). Mappable units include cratered plains, light plains, smooth dark plains, units associated with multi-ring structures, and other impact deposits. Figure 17.33 (see color plate) is a generalized photogeological map of these units, expanded from that of Bender *et al.* (1997a) using *Galileo* images to fill areas not observed by *Voyager* and drawing on new insights from higher resolution data (Greeley *et al.* 2000). Areas not covered by images with resolutions adequate for global-scale mapping (a few km/pixel or better) include about half of the south polar region, about one-eighth of the north polar region, and a few small, equatorial “gores” (coverage gaps). Stratigraphy discussed here is mainly based on superposition and cross-cutting relations rather than on relative crater densities. Crater statistics and age implications are discussed in Chapter 18, but the two extant models for the crater production history of Callisto both support an ancient age for the surface of >4 Gyr. The two models differ in the ages of younger large impact features however, with ages for Lofn ranging from 2 to 4 Gyr (Wagner *et al.* 1998 and Chapter 18).

Cratered plains materials, designated cp on the map, dominate Callisto. With average albedo ~ 0.2 , this unit is heavily cratered (Figure 17.10). Cratered plains represent the ancient lithosphere of Callisto, consisting of ice, rock, and dust, all brecciated and “gardened” by impact cratering and other erosional processes.

Light plains (unit lp on Figure 17.33) have higher albedos than cp and form circular, elliptical, or irregular patches (Bender *et al.* 1997a). They include palimpsests and typically have a relatively low density of superposed craters. Light plains are interpreted to be relatively ice-rich deposits excavated by impact processes. Circular or irregular, slightly brighter patches are mapped and interpreted here as highly degraded palimpsest remnants. Utgard is mapped by the presence of light plains, which could be central palimpsest deposits.

Smooth plains materials (unit sp on Figure 17.33) occur in association with multi-ring structure scarps. Some smooth plains associated with Valhalla were imaged at moderate resolution (410 m/pixel) on C9 (Figure 17.34); the images show higher albedo areas correlating with intensely fractured terrain, but with no evidence of the resurfacing that had been suspected after *Voyager*. Other apparent sp units, away from basin scarps, identified from *Voyager* images are no longer classified as sp, since higher resolution *Galileo* images reveal them to be swarms of knobs and other non-smooth terrains.

In addition to the light smooth plains, *Voyager* images show dark smooth areas within the cratered plains, once suggested to be possible cryovolcanic deposits (Remsburg 1981, Schenk 1995). In two cases imaged by *Galileo* on C20 and C21, the dark terrain appears smooth and slightly undulating. In C20 images (Figure 17.35), the dark terrain appears to mantle knobs and craters and embay surrounding terrain. Prockter *et al.* (1998a) discussed how similar dark deposits

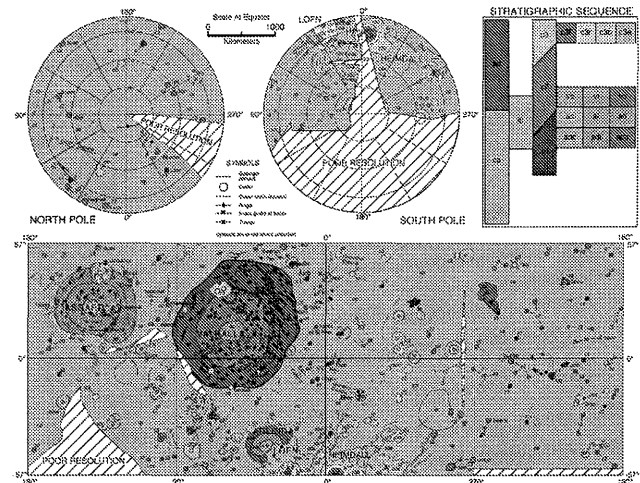


Figure 17.33. Geological sketch map of Callisto derived from that of Bender *et al.* (1997a) with additional mapping provided by *Galileo* imaging data: sp, lp, and cp refer to smooth plains, light plains, and cratered plains, respectively; c1, c2, and c3 refer to crater units, with c1 being oldest; c3 units are further subdivided into floor (f), rim (r), bright ejecta (b), and general ejecta (e) materials; units associated with Valhalla include central materials (vc), inner ring materials (vi) and outer ring materials (vo); Asgard multi-ring units include central materials (ac), inner ring materials (ai), and outer ring materials (ao); Adlinda multi-ring structure units include central materials (adi), and outer ring materials (ado). Greeley *et al.* (2000) subdivided crater deposits associated with Lofn and Heimdall into crater floor material (c3f), crater rim material (c3r), a bright ejecta facies (c3b), and general ejecta deposits (c3e). The distinction between the latter two units is that bright ejecta has a very high albedo, perhaps impact melt deposits rich in water ice, while the outer unit (c3e) may have been excavated from a shallower depth, hence containing more non-ice components, consistent with its lower albedo. At the time of going to press a colour version of this figure was available for download from <http://www.cambridge.org/9780521035453>.

might form on Ganymede. Moore *et al.* (1999) proposed that dark mantles were lag deposits created by sublimation disaggregation of bedrock, similar to an explanation offered by Prockter *et al.* (1998a), for the formation of dark deposits on Ganymede. A C21 image (Figure 17.19) shows small furrows and ridges, but no obvious flows or other features indicating cryovolcanic activity.

Following Greeley *et al.* (2000), multi-ring related units are mapped in Figure 17.33: the central zone materials and two encircling units for Valhalla (units vc, vi and vo), Asgard (units ac, ai, and ao), and Adlinda (units adc, adi, and ado). Central zone deposits (units vc, ac, and adc), with generally higher albedos due to greater ice content, are interpreted as material derived from the icy lithosphere by impact. Units vi, ai, and adi form the innermost encircling bands of fractured, lineated materials around the central zones of Valhalla, Asgard, and Adlinda, respectively. The outermost encircling units (vo, ao, and ado) have often sinuous grabens. This unit for Asgard (ao) could mark the extent of its continuous ejecta. The outer units for Valhalla (vo) and Adlinda (ao) might not represent continuous ejecta and could have been mapped (alternatively) as structurally deformed cratered plains, rather than as material units. In any event, the structures in the units are interpreted by Greeley



Figure 17.34. Moderate resolution (410 m/pixel) image of the Valhalla outer ring zone centered about 27° N, 27.3° W, showing sinuous grabens; smooth, light plains had been mapped on *Voyager* images in association with these structures. As seen here, the terrain to the east (right) of the main scarps is bright because of the numerous frosted knobs composing the small fractures associated with the grabens. (Mosaic of *Galileo* images from observation C9CSVALHAL01. North is up. Sun is from the left.)

et al. (2000) to reflect deformation and adjustment of the icy lithosphere following the multi-ring forming impacts.

Three classes of craters, based on their degradation state, are units c1, c2, and c3 (oldest to youngest). Classifications may not always be uniform, however, due to highly variable resolution, viewing and illumination geometry, etc. The best preserved craters, c3, have sharp rims, fresh ejecta blankets, and, in many cases, bright rays. C2 craters have fairly sharp rims, albedos similar to the background cratered plains, and sometimes indications of ejecta. C1 craters have degraded or partial rims, no detectable ejecta deposits, and tend to be flat-floored.

17.3.6 Interior

Repeated, very close flybys of Callisto by *Galileo* provide insight to its interior. Chapter 13 discusses the origin, thermal history, interior composition, structure, and evolution



Figure 17.35. Dark plains centered at 3.9° S, 189.2° W, imaged at 101 m/pixel by *Galileo* on orbit C20, showing mantling and embayment of older terrain. (Portion of *Galileo* image PICNO 20C0002, centered $\sim 4^{\circ}$ S, 189° W, North is up. Sun is low and from the left.)

of Callisto and the other Galilean satellites. We briefly summarize post-*Galileo* understanding of Callisto's interior here. Initial models of the interior derived from radio Doppler measurements of the gravity field (Anderson *et al.* 1998) suggest that Callisto is at least partially differentiated. If Callisto has a rock-metal core, it must be <25 percent of Callisto's radius, with an outer layer of clean ice <350 km thick. However, modeling ambiguities allow for an interior with ice and rock mixed all the way to Callisto's center (Anderson *et al.* 1998, 2001, Showman and Malhotra 1999). The discovery of Callisto's induced magnetic field indicates a conducting subsurface layer, perhaps a subsurface zone of liquid water ~ 10 km thick at a depth <300 km (Khurana *et al.* 1998, Kivelson *et al.* 1999) but probably >100 km (e.g., Ruiz 2001). Given Callisto's apparent lack of internal heating, implied by the lack of endogenic surface features, contaminants (e.g., salts or ammonia) may be required to depress the freezing point and permit such a layer of liquid to survive (e.g., Khurana *et al.* 1998, Stevenson 1998). Alternatively, highly anisotropic behavior of ice viscosity as a function of temperature, pressure, grain size, and stress may prevent ice overlying the liquid layer from convecting, thus inhibiting heat loss that would otherwise freeze the layer (e.g., Ruiz 2001).

What does the appearance of Callisto's surface imply for these models? The bright, icy centers of impact features like Lofn may indicate that a relatively clean-ice zone occurs

within a few kilometers of the surface, beneath relatively “dirty” material. Schenk (1995) proposed that at least the bedrock component of this “dirty” layer could have a “primordial” composition and be thought of as a ~ 5 km thick “crust” overlying a “mantle” of cleaner ice. He speculated that this “crust” might be laterally and vertically complex. Thermally induced segregation of “bedrock” into frosts and silicate-rich lag, both as a function of topography and latitude (Spencer 1987a, Moore *et al.* 1999), would presumably contribute to this heterogeneity. Spatial variations of SO_2 , CO_2 , and visible color could be due to large-scale primordial crustal compositional anisotropy (Hibbits *et al.* 2000). The abundance of SO_2 and CO_2 relative to Ganymede may be a consequence of the comparatively primordial composition of Callisto’s crust.

The formation of the many tectonic rings of multi-ringed impact features as well as the development of palimpsests and domes within craters imply that the ice “mantle” has, in the past, deformed plastically, at least down several tens of km. The concentric multi-ring impact faults are consistent with impacts into a “thin” brittle shell overlying a plastically deformable substrate, as proposed by McKinnon and Melosh (1980). Crater densities for various units associated with multi-ring structures show little variation, suggesting that they all formed in a short period of time, with little later resurfacing or fracturing, unlike evolution of lunar mare basins (Greeley *et al.* 2000). Post-*Voyager* proposals that many Callisto impact craters are “viscously relaxed” (e.g., Passey and Shoemaker 1982) must be revised due to recent studies of crater depth *vs.* diameter in icy targets, which indicate that such craters are formed intrinsically shallower than comparable-sized craters in silicate crust targets (e.g., Schenk 1991, 1995). Palimpsests and dome craters clearly indicate plastic deformation of the substrate (Chapter 18). All this evidence for past eras of plastic rheology of at least the upper tens of km of an icy “mantle” must be reconciled with models for a non-convecting ice layer that explain the surviving liquid zone >100 km beneath Callisto’s surface (Ruiz 2001).

17.4 CONCLUSIONS

Along with the discovery of Callisto’s conducting layer, major *Galileo* discoveries about Callisto include the complete absence of cryovolcanic resurfacing, the relatively undifferentiated interior, and the presence of massive landform erosion likely from sublimation processes. Callisto’s landscape at decameter scales is unique among the Galilean satellites, and might be most akin to that of cometary nuclei (Moore *et al.* 1999). The process of sublimation degradation, previously underappreciated, is now recognized as a major surface modification process on Callisto. Its role in mass wasting and landslide initiation appears elemental in creating the bizarre and astonishing scenery imaged by *Galileo*.

Outstanding questions remaining in Callisto studies must begin with what is the actual configuration of its interior? Is there a rock core? How is undifferentiated material distributed within Callisto’s interior? What is the composition and thickness of the liquid layer? Does it indeed exist, and, if so, and how has it survived to the present? Moving toward the surface, what is the structure of the “crust?” Is

the dark, non-icy material, so abundant on its surface, restricted to the upper several km? What is the composition of this non-icy material? Why is Callisto’s “crust” apparently so volatile-rich compared to its siblings? Why are there 100-km-scale heterogeneities in composition and albedo of the surface? Do we really understand why knobs with bright summits dominate the surface at decameter scale? What is the nature and origin of the leading–trailing hemisphere dichotomy in photometric properties? Why is there apparently a dearth of palimpsests relative to Ganymede? How do large impact ring structures vary with azimuth, radial distance, and overall scale, and what do they imply for Callisto’s interior (and by extension to the smaller structures on Europa, for ice shell/ocean combinations in general)? How do impact crater populations vary as a function of distance from the apex of motion, everywhere on Callisto? What are the roles of saturation equilibrium, viscous relaxation, sublimation degradation, and nonsynchronous rotation (and other possible lithospheric shifts) in determining these populations (and high resolution views of crater chains are important here)? And what are the retention ages represented by these crater counts? What is all of this telling us about Galilean satellite formation and evolution? And the biggest question: should we assume that the reason Callisto and Ganymede had divergent histories is solely the consequence of the role of tidal heating, or are there viable alternative explanations (such as accretion dynamics)?

Future exploration of Callisto will probably piggyback on missions to and through the jovian system. The currently planned *New Horizons* mission to Pluto/Charon and the Kuiper Belt may fly close enough in 2007 to obtain disk-resolved spectra of Callisto. Indeed, depending on the encounter geometry, Callisto may be studied at moderately high spatial resolutions by all remote-sensing instruments aboard that spacecraft.

The proposed Jupiter Icy Moons Orbiter (JIMO) is currently planned to first orbit Callisto then its two icy siblings, Ganymede and Europa. During the Callisto phase of the JIMO mission, globally complete mapping should be obtained, all at a nominal resolution of at 100 m/pixel or better. It would be desirable to map selected areas of high science interest at resolutions better than 10 m/pixel, preferably ~ 1 m/pixel. Spectroscopic studies should, in addition to good (better than 100 m/pixel) spatial resolution have sufficient spectral resolution and spectral range at high (>100) signal-to-noise at relevant wavelengths. A mid-IR imaging radiometer could map the thermo-physical properties of surface materials, such as their thermal inertia from which particle size could be derived. A far-IR or microwave radiometer, if sensitive enough, could conceivably make measurements from which Callisto’s heat flux might be determined. Careful measure of the orbits themselves will permit the detection of any mass anisostasy within Callisto’s interior, which would go far to resolving its degree of differentiation. Ground-penetrating radar, if available, would permit a measure of the segregation ice from non-ice and map the thickness of the refractory lag. Also, radar might reveal buried but surviving roots of ancient endogenic activity. Active energetic ionizing of surface materials with lasers or particle beams could potentially complement orbital compositional investigations. These are but a few examples of the ability of a comprehensive orbital study af-

forded by JIMO toward answering many of the outstanding questions remaining in Callisto studies.

If missions are mounted to specifically address outstanding questions of Callisto itself, in situ analysis by a lander/rover of the chemistry, mineralogy, and sedimentology of surface materials would resolve much of the ambiguity that will persist so long as studies of its surface are limited to remotely sensed observations. A landed geophysics network would greatly improve knowledge of both the shallow and deep interior. Callisto, once unknown and then disregarded after *Voyager*, has emerged in the post-*Galileo* era worthy of the same intense scientific scrutiny that is lavished upon her siblings, playing an essential role in our understanding of the evolution of icy moons, and in a larger sense, the grand tapestry of solar system history.

Acknowledgements. We thank Andrew J. Dombard and William B. McKinnon for significantly improving this chapter by their careful reviews. We especially thank both Pam Engebretson for her work on the figures and Carrie Chavez for her work on the text. This chapter was funded for the most part by the *Galileo* Project.

REFERENCES

- Anderson, J. D., G. Schubert, R. A. Jacobson, E. L. Lau, W. B. Moore, and W. L. Sjo Gren, Distribution of rock, metals, and ices in Callisto, *Science* **280**, 1573, 1998.
- Anderson, J. D., R. A. Jacobson, T. P. McElrath, W. B. Moore, G. Schubert, and P. C. Thomas, Shape, mean radius, gravity field, and interior structure of Callisto, *Icarus* **153**, 157–161, 2001.
- Asphaug, E., J. M. Moore, D. Morrison, P. H. Figueredo, R. Greeley, R. T. Pappalardo, L. M. Prockter, R. Tufts, and *Galileo* SSI Team, Crater-controlled fracture networks and the depth of ice lithospheres, in *Lunar and Planetary Science Conference Abstracts*, vol. 29, p. 1587, 1998.
- Basilevsky, A. T., Morphology of Callisto knobs from photogeologic analysis of *Galileo* SSI images taken at orbit C21, in *Lunar and Planetary Science Conference Abstracts*, vol. 33, p. 1014, 2002.
- Basilevsky, A. T., M. A. Ivanov, and V. P. Kryuchkov, On the degradation of impact craters on Callisto, *Astronomicheskii Vestnik* **34**, 277, 2000.
- Bender, K., J. Rice, D. Wilhelms, and R. Greeley, *Geology of Callisto 1:15 Million Geologic Map*, U.S. Geol. Surv. Misc. Investigations Series, **I-2581**, 1997a.
- Bender, K. C., K. C. Homan, R. Greeley, C. R. Chapman, J. Moore, C. Pilcher, W. J. Merline, J. W. Head, M. Belton, and T. V. Johnson, The Asgard and Valhalla regions: *Galileo's* new views of Callisto, in *Lunar and Planetary Science Conference Abstracts*, vol. 28, p. 89, 1997b.
- Bierhaus, E. B., C. R. Chapman, W. J. Merline, R. Greeley, and J. Klemaszewski, Small crater populations on Callisto, in *Lunar and Planetary Science Conference Abstracts*, vol. 31, p. 1996, 2000.
- Black, G. J., D. B. Campbell, and P. D. Nicholson, Icy Galilean satellites: Modeling radar reflectivities as a coherent backscatter effect, *Icarus* **151**, 167–180, 2001a.
- Black, G. J., D. B. Campbell, and S. J. Ostro, Icy Galilean satellites: 70 cm radar results from Arecibo, *Icarus* **151**, 160–166, 2001b.
- Browning, L. B., M. E. Zolensky, and R. Barrett, Serpentine and modal compositions of CM chondrites, in *Lunar and Planetary Science Conference Abstracts*, vol. 22, p. 145, 1991.
- Brunsdon, D., Mass movements, in *Progress in Geomorphology*, C. E. Embleton and J. B. Thornes (eds), Arnold, 1979.
- Bulmer, M., *An Examination of Small Volcanoes in the Plains of Venus; with Particular Reference to the Evolution of Domes*, Ph.D. thesis, University of London, 1994.
- Buratti, B. J., Ganymede and Callisto: Surface textural dichotomies and photometric analysis, *Icarus* **92**, 312–323, 1991.
- Burgdorf, M. J., T. Encrenaz, J. R. Brucato, H. Feuchtgruber, G. R. Davis, E. Lellouch, B. M. Swinyard, T. G. Müller, S. D. Sidher, P. Morris, M. J. Griffin, L. Colangeli, and V. Menella, The emissivity of Mars and Callisto in the far infrared, *ISO Beyond the Peaks: The 2nd ISO Workshop on Analytical Spectroscopy*, A. Salama, M. F. Kessler, K. Leech and B. Schulz (eds), ESA-SP 456, 9, 2000.
- Calvin, W. M. and R. N. Clark, Modeling the reflectance spectrum of Callisto: 0.25 to 4.1 microns, *Icarus* **89**, 305–317, 1991.
- Calvin, W. M. and R. N. Clark, Spectral distinctions between the leading and trailing hemispheres of Callisto: New observations, *Icarus* **104**, 69–78, 1993.
- Calvin, W. M., R. N. Clark, R. H. Brown, and J. R. Spencer, Spectra of the icy Galilean satellites from 0.2 to 5 micron: A compilation, new observations, and a recent summary, *J. Geophys. Res.* **100**, 19041–19048, 1995.
- Carlson, R., W. Smythe, K. Baines, E. Barbinis, K. Becker, R. Burns, S. Calcutt, W. Calvin, R. Clark, G. Danielson, A. Davies, P. Drossart, T. Encrenaz, F. Fanale, J. Granahan, G. Hansen, P. Herrera, C. Hibbitts, J. Hui, P. Irwin, T. Johnson, L. Kamp, H. Kieffer, F. Leader, E. Lellouch, R. Lopes-Gautier, D. Matson, T. McCord, R. Mehlman, A. Ocampo, G. Orton, M. Roos-Serote, M. Segura, J. Shirley, L. Soderblom, A. Stevenson, F. Taylor, J. Torson, A. Weir, and P. Weissman, Near-infrared spectroscopy and spectral mapping of Jupiter and the Galilean satellites: Results from *Galileo's* initial orbit, *Science* **274**, 385–388, 1996.
- Carlson, R. W., A tenuous carbon dioxide atmosphere on Jupiter's moon Callisto, *Science* **283**, 820, 1999.
- Carr, M. H., M. J. S. Belton, K. Bender, H. Breneman, R. Greeley, J. W. Head, K. P. Klaassen, A. S. McEwen, J. M. Moore, S. Murchie, R. T. Pappalardo, J. Plutchak, R. Sullivan, G. Thornhill, and J. Veverka, The *Galileo* Imaging Team plan for observing the satellites of Jupiter, *J. Geophys. Res.* **100**, 18935–18956, 1995.
- Chapman, C. R. and W. B. McKinnon, Cratering of planetary satellites, in *Satellites*, J. A. Burns, M. S. Matthews (eds), University of Arizona Press, pp. 492–580, 1986.
- Chapman, C. R., J. Veverka, M. J. S. Belton, G. Neukum, and D. Morrison, Cratering on Gaspra, *Icarus* **120**, 231–245, 1996.
- Chapman, C. R., W. J. Merline, B. Bierhaus, S. Brooks, and *Galileo* Imaging Team, Cratering in the jovian system: Inter-satellite comparisons, in *Lunar and Planetary Science Conference Abstracts*, vol. 29, p. 1927, 1998.
- Chapman, C. R., B. Bierhaus, W. J. Merline, R. Greeley, J. Klemaszewski, and *Galileo* Imaging Team, Low spatial density of small craters on Callisto, *BAAS* **31**, 0, 1999.
- Chuang, F. C. and R. Greeley, Large mass movements on Callisto, *J. Geophys. Res.* **105**, 20227–20244, 2000.
- Clark, R. N., Ganymede, Europa, Callisto, and Saturn's rings: Compositional analysis from reflectance spectroscopy, *Icarus* **44**, 388–409, 1980.
- Clark, R. N., The spectral reflectance of water–mineral mixtures at low temperatures, *J. Geophys. Res.* **86**, 3074–3086, 1981.
- Clark, R. N. and P. G. Lucey, Spectral properties of ice-particulate mixtures and implications for remote sensing: I. Intimate mixtures, *J. Geophys. Res.* **89**, 6341–6348, 1984.
- Clark, R. N. and T. B. Mc Cord, The Galilean satellites: New

- near-infrared spectral reflectance measurements (0.65–2.5 microns) and a 0.325–5 micron summary, *Icarus* **41**, 323–339, 1980.
- Clark, R. N., R. B. Singer, P. D. Owensby, and F. P. Fanale, Galilean satellites: High precision near infrared spectrophotometry (0.65–2.5 μm) of the leading and trailing sides, *BAAS* **12**, 713, 1980.
- Clark, R. N., F. P. Fanale, and A. P. Zent, Frost grain size metamorphism: Implications for remote sensing of planetary surfaces, *Icarus* **56**, 233–245, 1983.
- Clark, R. N., F. P. Fanale, and M. J. Gaffey, Surface composition of natural satellites, in *Satellites*, J. A. Burns, M. S. Matthews (eds), University of Arizona Press, pp. 437–491, 1986.
- Colwell, J. E., B. M. Jakosky, B. J. Sandor, and S. A. Stern, Evolution of topography on comets: II. Icy craters and trenches, *Icarus* **85**, 205–215, 1990.
- Colwell, J. E., M. Horányi, and E. Grün, Jupiter's exogenic dust ring, *J. Geophys. Res.* **103**, 20 023–20 030, 1998.
- Cooper, J. F., R. E. Johnson, B. H. Mauk, H. B. Garrett, and N. Gehrels, Energetic ion and electron irradiation of the icy Galilean satellites, *Icarus* **149**, 133–159, 2001.
- Dalton, J. B. I., *Constraints on the Surface Composition of Jupiter's Moon Europa Based on Laboratory and Spacecraft Data*, Ph.D. thesis, University of Colorado, 2000.
- Davies, M. E., T. R. Colvin, J. Oberst, W. Zeitler, P. Schuster, G. Neukum, A. S. McEwen, C. B. Phillips, P. C. Thomas, J. Veverka, M. J. S. Belton, and G. Schubert, The control networks of the Galilean satellites and implications for global shape, *Icarus* **135**, 372–376, 1998.
- de Pater, I., B. L. Ulich, E. Kreysa, and R. Chini, Planetary observations at a wavelength of 355 microns, *Icarus* **79**, 190–195, 1989.
- Delitsky, M. L. and A. L. Lane, Chemical schemes for surface modification of icy satellites: A road map, *BAAS* **29**, 985, 1997.
- Delitsky, M. L. and A. L. Lane, Ice chemistry on the Galilean satellites, *J. Geophys. Res.* **103**, 31 391–31 404, 1998.
- Denk, T., G. Neukum, T. B. McCord, G. B. Hansen, C. A. Hibbitts, P. D. Martin, and Galileo SSI Team, Candidate surface materials of the icy Galilean satellites that might be distinguished by the Galileo SSI camera, in *Lunar and Planetary Science Conference Abstracts*, vol. 29, p. 1676, 1998.
- Dollfus, A. and E. Bowell, Polarimetric properties of the Lunar surface and its interpretation: Part I. Telescopic observations, *A&A* **10**, 29, 1971.
- Dombard, A. J., *Modeling of Geodynamical Processes on Ganymede and Callisto: Insight into Thermal and Tectonic Histories*, Ph.D. thesis, University of Washington, St. Louis, 2000.
- Domingue, D. L., A. L. Sprague, and D. M. Hunten, Dependence of mercurian atmospheric column abundance estimations on surface-reflectance modeling, *Icarus* **128**, 75–82, 1997.
- Fanale, F. P., R. H. Brown, D. P. Cruikshank, and R. N. Clark, Significance of absorption features in Io's IR reflectance spectrum, *Nature* **280**, 761–763, 1979.
- Gault, D. E., Saturation and equilibrium conditions for impact cratering on the lunar surface: Criteria and implications, *Radio Science* **5**, 273–291, 1970.
- Geiss, J., G. Gloeckler, H. Balsiger, L. A. Fisk, A. B. Galvin, F. Gliem, D. C. Hamilton, F. M. Ipavich, S. Livi, and U. Mall, Plasma composition in Jupiter's magnetosphere: Initial results from the Solar Wind Ion Composition Spectrometer, *Science* **257**, 1535–1539, 1992.
- Grün, E., H. Krüger, A. L. Graps, D. P. Hamilton, A. Heck, G. Linkert, H. A. Zook, S. Dermott, H. Fechtig, B. A. Gustafson, M. S. Hanner, M. Horányi, J. Kissel, B. A. Lindblad, D. Linkert, I. Mann, J. A. M. McDonnell, C. Morfill, G. E. and Polansky, G. Schwehm, and R. Srama, Galileo ob- serves electromagnetically coupled dust in the jovian magnetosphere, *J. Geophys. Res.* **103**, 20 011–20 022, 1998.
- Greeley, R., J. E. Klemaszewski, and R. Wagner, Galileo views of the geology of Callisto, *Planet. Space Sci.* **48**, 829–853, 2000.
- Greeley, R., S. Heiner, and J. E. Klemaszewski, Geology of Lofn Crater, Callisto, *J. Geophys. Res.* **106**, 3261–3274, 2001.
- Grundy, W. M., M. W. Buie, J. A. Stansberry, J. R. Spencer, and B. Schmitt, Near-infrared spectra of icy outer solar system surfaces: Remote determination of H₂O ice temperatures, *Icarus* **142**, 536–549, 1999.
- Hanel, R., B. Conrath, M. Flasar, L. Herath, V. Kunde, P. Lowman, W. Maguire, J. Pearl, J. Pirraglia, and L. Horn, Infrared observations of the jovian system from *Voyager 2*, *Science* **206**, 952–956, 1979.
- Hapke, B., Coherent backscatter and the radar characteristics of outer planet satellites, *Icarus* **88**, 407–417, 1990.
- Harcke, L. J., B. J. Butler, H. A. Zebker, M. A. Slade, and R. F. Jurgens, Unambiguous 3.5 cm radar images of Ganymede and Callisto from bistatic Goldstone/VLA radar observations, *BAAS* **33**, 0, 2001.
- Hendrix, A. R., C. A. Barth, C. W. Hord, A. L. Lane, W. K. Tobiska, and K. E. Simmons, Disk-resolved observations of the ultraviolet absorber on Callisto's leading hemisphere, in *Lunar and Planetary Science Conference Abstracts*, vol. 29, p. 1865, 1998.
- Hendrix, A. R., C. A. Barth, A. I. F. Stewart, C. W. Hord, and A. L. Lane, Hydrogen peroxide on the icy Galilean satellites, in *Lunar and Planetary Science Conference Abstracts*, vol. 30, p. 2043, 1999.
- Hibbitts, C. A., T. B. McCord, and G. B. Hansen, Distributions of CO₂ and SO₂ on the surface of Callisto, *J. Geophys. Res.* **105**, 22 541–22 558, 2000.
- Hibbitts, C. A., T. B. McCord, and G. B. Hansen, The non-ice material on Callisto, *Eos* p. B495, 2001a.
- Hibbitts, C. A., R. Pappalardo, J. Klemaszewski, T. B. McCord, and G. B. Hansen, Comparing carbon dioxide distributions on Ganymede and Callisto, in *Lunar and Planetary Science Conference Abstracts*, vol. 32, p. 1263, 2001b.
- Hibbitts, C. A., J. E. Klemaszewski, T. B. McCord, G. B. Hansen, and R. Greeley, CO₂-rich impact craters on Callisto, in *J. Geophys. Res.*, pp. 14–1, 2002.
- Hobbs, P. V., *Ice Physics*, Clarendon Press, 1974.
- Homan, K., K. Bender, J. Klemaszewski, R. Greeley, J. Head, R. Pappalardo, L. Prockter, and the Galileo Imaging Team, Multiring structures on Callisto: New views from Galileo, *Eos* p. F419, 1997.
- James, P. B., H. H. Kieffer, and D. A. Paige, The seasonal cycle of carbon dioxide on Mars, in *Mars*, pp. 934–968, 1992.
- Johnson, R. E., *Energetic Charged-Particle Interactions with Atmospheres and Surfaces*, Springer-Verlag, 1990.
- Johnson, T. V. and F. P. Fanale, Optical properties of carbonaceous chondrites and their relationship to asteroids, *J. Geophys. Res.* **78**, 8507–8518, 1973.
- Khurana, K. K., M. G. Kivelson, D. J. Stevenson, G. Schubert, C. T. Russell, S. Walker, R. J. and Joy, and C. Polansky, Induced magnetic fields as evidence for subsurface oceans in Europa and Callisto, *Nature* **395**, 777–780, 1998.
- Kieffer, H. H., Near Infrared Spectral Reflectance of Simulated Martian Frosts, 1968.
- Kieffer, H. H. and W. D. Smythe, Comparison with Jupiter's satellites, *Icarus* **21**, 506, 1974.
- King, T. V. V. and R. N. Clark, Spectral characteristics of chlorites and Mg-serpentines using high-resolution reflectance spectroscopy, *J. Geophys. Res.* **94**, 13 997–14 008, 1989.
- Kivelson, M. G., K. K. Khurana, D. J. Stevenson, L. Bennett, S. Joy, C. T. Russell, R. J. Walker, C. Zimmer, and C. Polansky, Europa and Callisto: Induced or intrinsic fields in a periodically varying plasma environment, *J. Geo-*

- phys. Res.* **104**, 4609–4626, 1999.
- Klemaszewski, J., J. Moore, E. Asphaug, D. Morrison, R. Greeley, R. Sullivan, P. Geissler, C. Chapman, P. Pilcher, W.-H. Ip, and the *Galileo* SSI Team, Exogenic degradation and mass wasting on the icy Galilean satellites, *Geol. Soc. Amer.* **29**, 314, 1997.
- Klemaszewski, J., R. Wagner, R. Greeley, G. Neukum, C. Chapman, W. Merline, and the *Galileo* SSI Team, Callisto multiring structures and large impactor populations from *Galileo* data, *Annal. Geophys.* **16**, 992, 1998a.
- Klemaszewski, J. E., R. Greeley, K. S. Homan, K. C. Bender, F. C. Chuang, S. Kadel, R. J. Sullivan, C. Chapman, W. J. Merline, J. Moore, R. Wagner, T. Denk, G. Neukum, J. Head, R. Pappalardo, L. Prockter, M. Belton, T. V. Johnson, C. Pilcher, and *Galileo* SSI Team, *Galileo* at Callisto: Overview of nominal mission results, in *Lunar and Planetary Science Conference Abstracts*, vol. 29, p. 1866, 1998b.
- Kliore, A. J., A. Anabtawi, A. F. Nagy, and *Galileo* Radio Propagation Science Team, The ionospheres of Ganymede and Callisto from *Galileo* radio occultations, *BAAS* **33**, 0, 2001.
- Lane, A. L. and D. L. Domingue, IUE's view of Callisto: Detection of an SO₂ absorption correlated to possible torus neutral wind alterations, *Geophys. Res. Lett.* **24**, 1143, 1997.
- Lebofsky, L. A., Stability of frosts in the solar system, *Icarus* **25**, 205–217, 1975.
- Lewis, J. S., Low temperature condensation from the solar nebula, *Icarus* **16**, 241, 1972a.
- Lewis, J. S., Metal/silicate fractionation in the solar system, *Earth Planet. Sci. Lett.* **15**, 286–290, 1972b.
- Malin, M. C., Mass movements on Venus: Preliminary results from Magellan cycle 1 observations, *J. Geophys. Res.* **97**, 16 337, 1992.
- Martin, T. Z., J. D. Goguen, L. D. Travis, L. K. Tamppari, L. Barnard, and L. Doose, *Galileo* PPR polarimetric phase curves for the Galilean satellites, *BAAS* **32**, 0, 2000.
- McCaughey, J. F., L. A. Soderblom, and B. A. Smith, Erosional scarps on Io, *Nature* **280**, 736–738, 1979.
- McCord, T. B., R. Carlson, W. Smythe, G. Hansen, R. Clark, C. Hibbitts, F. Fanale, J. Granahan, M. Segura, D. Matson, T. Johnson, and P. Martin, Organics and other molecules in the surfaces of Callisto and Ganymede, *Science* **278**, 271–275, 1997.
- McCord, T. B., G. B. Hansen, R. N. Clark, P. D. Martin, C. A. Hibbitts, F. P. Fanale, J. C. Granahan, M. Segura, D. L. Matson, T. V. Johnson, R. W. Carlson, W. D. Smythe, and G. E. Danielson, Non-water-ice constituents in the surface material of the icy Galilean satellites from the *Galileo* Near Infrared Mapping Spectrometer investigation, *J. Geophys. Res.* **103**, 8603–8626, 1998.
- McCord, T. B., R. H. Brown, K. Baines, G. Bellucci, J. Bibring, B. Buratti, F. Capaccioni, P. Cerroni, R. Clark, A. Coradini, D. Cruikshank, P. Drossar, V. Formisano, R. Jaumann, Y. Langevin, D. Matson, V. Mennella, R. Nelson, P. Nicholson, B. Sicardy, C. Sotin, G. Hanson, and C. Hibbitts, Galilean satellite surface composition: New *Cassini* VIMS observations and comparison with *Galileo* NIMS measurements, in *Eos*, pp. B504+, 2001.
- McDonald, G. D., CH₄/NH₃/H₂O spark tholin: Chemical analysis and interaction with jovian aqueous clouds, *Icarus* **94**, 354–367, 1991.
- McDonald, G. D., L. J. Whited, C. Deruiter, B. N. Khare, A. Patnaik, and C. Sagan, Production and chemical analysis of cometary ice tholins, *Icarus* **122**, 107–117, 1996.
- McEwen, A. S., Mobility of large rock avalanches: Evidence from Valles Marineris, Mars, *Geology* **17**, 1111–1114, 1989.
- McGee, W. J., Sheetflood erosion, *Geol. Soc. Amer. Bull.* **8**, 87, 1897.
- McKinnon, W. B. and H. J. Melosh, Evolution of planetary lithospheres: Evidence from multiringed structures on Ganymede and Callisto, *Icarus* **44**, 454–471, 1980.
- McKinnon, W. B. and E. M. Parmentier, Ganymede and Callisto, in *IAU Colloq. 77: Some Background about Satellites*, pp. 718–763, 1986.
- Melosh, H. J., Global tectonics of a despun planet, *Icarus* **31**, 221–243, 1977.
- Melosh, H. J., *Impact Cratering: A Geologic Process*, Research supported by NASA. New York, Oxford University Press (Oxford Monographs on Geology and Geophysics, No. 11), 1989.
- Merline, W. J., C. R. Chapman, B. Bierhaus, S. Brooks, J. Moore, J. E. Klemaszewski, R. Greeley, and *Galileo* Imaging Team, Cratering on Callisto from the *Galileo* Prime Mission, *BAAS* **30**, 1122, 1998.
- Merrill, R. B. and P. H. Schultz, eds, *Multi-Ring Basins: Formation and Evolution*, 1981.
- Moore, J. M., M. T. Mellon, and A. P. Zent, Mass wasting and ground collapse in terrains of volatile-rich deposits as a solar system-wide geological process: The pre-*Galileo* view, *Icarus* **122**, 63–78, 1996.
- Moore, J. M., E. Asphaug, D. Morrison, J. R. Spencer, C. R. Chapman, B. Bierhaus, R. J. Sullivan, F. C. Chuang, J. E. Klemaszewski, R. Greeley, K. C. Bender, P. E. Geissler, P. Helfenstein, and C. B. Pilcher, Mass movement and landform degradation on the icy Galilean satellites: Results of the *Galileo* Nominal Mission, *Icarus* **140**, 294–312, 1999.
- Moore, M. H. and R. L. Hudson, IR detection of H₂O₂ at 80 K in ion-irradiated laboratory ices relevant to Europa, *Icarus* **145**, 282–288, 2000.
- Morrison, D., Radiometry of satellites and of the rings of Saturn, in *Planetary Satellites*, J. A. Burns (ed), University of Arizona Press, pp. 269–301, 1977.
- Morrison, D. and J. A. Burns, The jovian satellites, in *Jupiter*, T. Gehrels (ed), University of Arizona Press, pp. 991–1034, 1976.
- Morrison, D. and D. P. Cruikshank, Thermal properties of the Galilean satellites, *Icarus* **18**, 224, 1973.
- Morrison, D., Introduction to the satellites of Jupiter, in *Satellites of Jupiter*, Morrison, D. and M. S. Matthews, eds, University of Arizona Press, 1982.
- Morrison, D. and N. D. Morrison, Photometry of the Galilean satellites, in *Planetary Satellites*, J. A. Burns (ed), University of Arizona Press, pp. 363–378, 1977.
- Morrison, D., N. D. Morrison, and A. R. Lazarewicz, Four-color photometry of the Galilean satellites, *Icarus* **23**, 399–416, 1974.
- Muhleman, D. O. and G. L. Berge, Observations of Mars, Uranus, Neptune, Io, Europa, Ganymede, and Callisto at a wavelength of 2.66 mm, *Icarus* **92**, 263–272, 1991.
- Murchie, S. L., J. W. Head, and J. B. Plescia, Tectonic and volcanic evolution of dark terrain and its implications for the internal structure and evolution of Ganymede, *J. Geophys. Res.* **95**, 10 743–10 768, 1990.
- Noll, K. S., R. E. Johnson, M. A. McGrath, and J. J. Caldwell, Detection of SO₂ on Callisto with the Hubble Space Telescope, *Geophys. Res. Lett.* **24**, 1139, 1997.
- Ostro, S. J., D. B. Campbell, R. A. Simpson, R. S. Hudson, J. F. Chandler, K. D. Rosema, I. I. Shapiro, E. M. Standish, R. Winkler, and D. K. Yeomans, Europa, Ganymede, and Callisto: New radar results from Arecibo and Goldstone, *J. Geophys. Res.* **97**, 18 227, 1992.
- Passey, Q. R. and E. M. Shoemaker, Craters and basins on Ganymede and Callisto: Morphological indicators of crustal evolution, in *Satellites of Jupiter*, D. Morrison and M. S. Matthews (eds), University of Arizona Press, pp. 379–434, 1982.
- Peters, K., The coherent backscattering effect: A vector

- formulation accounting for polarization and absorption effects and small and large scatterers, *Phys. Rev. B* **42**, 801–812, 1992.
- Pilcher, C. B., S. T. Ridgeway, and T. B. McCord, Galilean satellites: Identification of water frost, *Science* **178**, 1087–1089, 1972.
- Pollack, J. B., F. C. Witteborn, E. F. Erickson, D. W. Strecker, B. J. Baldwin, and T. E. Bunch, Near-infrared spectra of the Galilean satellites: Observations and compositional implications, *Icarus* **36**, 271–303, 1978.
- Prockter, L. M., J. W. Head, R. T. Pappalardo, E. Asphaug, and Galileo SSI Team, Geology of Nicholson Regio from Galileo imaging: Evidence for tectonic focusing through craters, in *Lunar and Planetary Science Conference Abstracts*, vol. 29, p. 1336, 1998a.
- Prockter, L. M., J. W. Head, R. T. Pappalardo, D. A. Senske, G. Neukum, R. Wagner, U. Wolf, J. O. Oberst, B. Giese, J. M. Moore, C. R. Chapman, P. Helfenstein, R. Greeley, H. H. Breneman, and M. J. S. Belton, Dark terrain on Ganymede: Geological mapping and interpretation of Galileo Regio at high resolution, *Icarus* **135**, 317–344, 1998b.
- Purves, N. G. and C. B. Pilcher, Thermal migration of water on the Galilean satellites, *Icarus* **43**, 51–55, 1980.
- Remsberg, A. R., A structural analysis of Valhalla Basin, Callisto, in *Lunar and Planetary Science Conference Abstracts*, vol. 12, pp. 874–876, 1981.
- Rogers, J. H., *The Giant Planet Jupiter*, Cambridge University Press, 1995.
- Rosenbush, V. K., V. V. Avramchuk, A. E. Rosenbush, and M. I. Mishchenko, Polarization properties of the Galilean satellites of Jupiter: Observations and preliminary analysis, *ApJ* **487**, 402, 1997.
- Roush, T. L., J. B. Pollack, F. C. Witteborn, J. D. Bregman, and J. P. Simpson, Ice and minerals on Callisto: A reassessment of the reflectance spectra, *Icarus* **86**, 355–382, 1990.
- Ruiz, J., The stability against freezing of an internal liquid-water ocean in Callisto, *Nature* **412**, 409–411, 2001.
- Schenk, P., W. McKinnon, and J. Moore, Stereo Topography of Valhalla and Gilgamesh, in *Lunar and Planetary Science Conference Abstracts*, vol. 28, p. 1249, 1997.
- Schenk, P. M., Ganymede and Callisto: Complex crater formation and planetary crusts, *J. Geophys. Res.* **96**, 15 635, 1991.
- Schenk, P. M., Central pit and dome craters: Exposing the interiors of Ganymede and Callisto, *J. Geophys. Res.* **98**, 7475–7498, 1993.
- Schenk, P. M., The Geology of Callisto, *J. Geophys. Res.* **100**, 19 023–19 040, 1995.
- Schenk, P. M., Thickness constraints on the icy shells of the Galilean satellites from a comparison of crater shapes, *Nature* **417**, 419–421, 2002.
- Schenk, P. M. and M. H. Bulmer, Origin of mountains on Io by thrust faulting and large-scale mass movements, *Science* **279**, 1514, 1998.
- Schenk, P. M. and W. B. McKinnon, Ring geometry on Ganymede and Callisto, *Icarus* **72**, 209–234, 1987.
- Schenk, P. M. and F. J. Ridolfi, Morphology and scaling of ejecta deposits on icy satellites, *Geophys. Res. Lett.* **29**, 31–1, 2002.
- Sharp, R. P., Mars: Fretted and chaotic terrains, *J. Geophys. Res.* **78**, 4073–4083, 1973a.
- Sharp, R. P., Mars: South polar pits and etched terrain, *J. Geophys. Res.* **78**, 4222–4230, 1973b.
- Sharpe, C., *Landslides and Related Phenomena*, Cooper Square, 1939.
- Shoemaker, E. M., B. K. Lucchitta, D. E. Wilhelms, J. B. Plescia, and S. W. Squyres, The Geology of Ganymede, in *Satellites of Jupiter*, D. Morrison and M. S. Matthews (eds), University of Arizona Press, pp. 435–520, 1982.
- Showman, A. and R. Malhotra, The Galilean satellites, *Science* **286**, 77–84, 1999.
- Sieger, M. T., W. C. Simpson, and T. M. Orlando, Production of O₂ on icy surfaces by electronic excitation of low-temperature water ice, *Nature* **394**, 554–556, 1998.
- Smith, B. A., L. A. Soderblom, R. Beebe, J. Boyce, G. Briggs, M. Carr, S. A. Collins, T. V. Johnson, A. F. Cook, G. E. Danielson, and D. Morrison, The Galilean satellites and Jupiter: *Voyager 2* imaging science results, *Science* **206**, 927–950, 1979a.
- Smith, B. A., L. A. Soderblom, T. V. Johnson, A. P. Ingersoll, S. A. Collins, E. M. Shoemaker, G. E. Hunt, H. Masursky, M. H. Carr, M. E. Davies, A. F. Cook, J. M. Boyce, T. Owen, G. E. Danielson, C. Sagan, R. F. Beebe, J. Veverka, J. F. McCauley, R. G. Strom, D. Morrison, G. A. Briggs, and V. E. Suomi, The Jupiter system through the eyes of *Voyager 1*, *Science* **204**, 951–957, 1979b.
- Smythe, W. D., R. M. Nelson, and D. B. Nash, Spectral evidence for SO₂ frost or adsorbate on Io's surface, *Nature* **280**, 766, 1979.
- Soderblom, L. A., A model for small-impact erosion applied to the lunar surface, *J. Geophys. Res.* **75**, 2655–2661, 1970.
- Spencer, J. R., *The Surfaces of Europa, Ganymede, and Callisto: An Investigation Using Voyager IRIS Thermal Infrared Spectra*, Ph.D. thesis, University of Arizona, 1987a.
- Spencer, J. R., Thermal segregation of water ice on the Galilean satellites, *Icarus* **69**, 297–313, 1987b.
- Spencer, J. R., A rough-surface thermo-physical model for airless planets, *Icarus* **83**, 27–38, 1990.
- Spencer, J. R. and P. R. Maloney, Mobility of water ice on Callisto: Evidence and implications, *Geophys. Res. Lett.* **11**, 1223–1226, 1984.
- Spencer, J. R., L. K. Tamppari, T. Z. Martin, and L. D. Travis, Temperatures on Europa from Galileo PPR: Nighttime thermal anomalies, *Science* **284**, 1514–1516, 1999.
- Spudis, P. D., *The Geology of Multi-Ring Impact Basins*, Cambridge University Press, 1993.
- Squyres, S. W., Surface temperatures and retention of H₂O frost on Ganymede and Callisto, *Icarus* **44**, 502–510, 1980.
- Stebbins, J. and T. S. Jacobsen, Further photometric measures of Jupiter's satellites and Uranus, with tests for the solar constant, *Lick Observatory Bulletin* **13**, 180–195, 1928.
- Stephenson, P., Some considerations of snow metamorphism in the antarctic ice sheet in the light ice crystal studies, in *Physics of Snow and Ice*, H. Oura (ed.), pp. 725–740, Hokkaido University, 1967.
- Stevenson, D., An ocean within Callisto?, *Eos* **79**, F535, 1998.
- Thomas, P. G. and P. L. Masson, Tectonics of Valhalla Basin on Callisto, in *NATO ASIC Proc. 156: Ices in the Solar System*, p. 781, 1985.
- Thompson, D. T. and G. W. Lockwood, Photoelectric photometry of Europa and Callisto 1976–1991, *J. Geophys. Res.* **97**, 14 761, 1992.
- Varnes, D., Landslide types and processes, in *Landslides and Engineering Practice*, E. B. Eckel (ed.), pp. 20–47, National Academy of Sciences, 1958.
- Veverka, J., Photometry of satellite surfaces, in *Planetary Satellites*, J. A. Burns (ed.), University of Arizona Press, pp. 171–209, 1977a.
- Veverka, J., Polarimetry of satellite surfaces, in *Planetary Satellites*, J. A. Burns (ed.), University of Arizona Press, pp. 210–230, 1977b.
- Wagner, R. and G. Neukum, Photogeologic units and fracture systems in the equatorial and midlatitude regions of Callisto, in *Lunar and Planetary Science Conference Abstracts*, vol. 22, p. 1453, 1991.
- Wagner, R. and G. Neukum, Surface units on Callisto: A pre-Galileo view, *BAAS* **26**, 1162, 1994.

- Wagner, R., U. Wolf, G. Neukum, T. Denk, and the *Galileo* SSI Team, Time-stratigraphy of Callisto's dark terrain and of major basins as observed by *Voyager* and the *Galileo* SSI imaging experiment, *Eos* **78**, 420, 1997.
- Wagner, R., U. Wolf, G. Neukum, J. E. Klemaszewski, R. Greeley, and *Galileo* Imaging Team, Time-stratigraphy and crater retention ages of geologic units on Callisto, in *Lunar and Planetary Science Conference Abstracts*, vol. 29, p. 1918, 1998.
- Wagner, R., U. Wolf, G. Neukum, and the *Galileo* SSI Team, Ages of individual craters on the Galilean satellites Ganymede and Callisto, in *Lunar and Planetary Science Conference Abstracts*, vol. 30, p. 1818, 1999.
- Wagner, R., G. Neukum, R. Greeley, J. E. Klemaszewski, and the *Galileo* Imaging Team, Fractures, scarps, and lineaments on Callisto and their correlation with surface degradation, in *Lunar and Planetary Science Conference Abstracts*, vol. 32, p. 1838, 2001.
- Wagner, R. J., U. Wolf, G. Neukum, R. Greeley, J. E. Klemaszewski, and *Galileo* SSI Team, Callisto during the *Galileo* Europa Mission (GEM): II. Geology and stratigraphy of the C21 target area, in *Lunar and Planetary Science Conference Abstracts*, vol. 31, p. 1955, 2000.
- Warren, S. G., Optical constants of ice from the ultraviolet to the microwave, *Appl. Opt.* **23**, 1206–1225, 1984.
- Watts, A., R. Greeley, and H. J. Melosh, Formation of antipodal terrains on icy satellites, in *Lunar and Planetary Science Conference Abstracts*, vol. 20, p. 1183, 1989.
- Winter, D. F. and J. A. Krupp, Directional characteristics of infrared emission from the Moon, *Moon* **2**, 279–292, 1971.